detectable at 20 weeks of age (Fig. 2A). Together, our results indicate that hUCH-L1^{I93M} is expressed in the neurons of the substantia nigra in H-hI93M mice, but the number of positive cells declines before 20 weeks of age. With the failure to detect hUCH-L1 protein in hWT/*gad* mice and L-hI93M/*gad* mice both in the Western blotting and the immunohistochemistry, we performed most of the analysis using H-hI93M mice with non-Tg mice as a control.

3.2. Loss of dopaminergic neurons in the substantia nigra of 20-week-old H-hI93M mice

We next determined whether the number of midbrain dopaminergic neurons was reduced in the substantia nigra of transgenic mice using TH immunohistochemistry. The number of TH-positive dopaminergic neurons in the substantia nigra at the same neuroanatomical level was compared and quantified for each transgenic mouse line. Surprisingly, we detected an ~30% reduction in TH-positive neurons in 20-week-old H-hI93M mice as compared with those in non-Tg control mice (Fig. 3A and B). This reduction was not seen in 12-week-old H-hI93M mice or 20-week-old L-hI93M mice. Together with the decrease in the level of UCH-L1^{I93M} (Fig. 1B) and the reduction in UCH-L1-positive neurons in the substantia nigra of H-hI93M/*gad* mice, our data indicate that UCH-L1^{I93M} expression in the dopaminergic neurons is sufficient to induce the degeneration of these neurons.

MPTP is a toxin used to induce an acute Parkinsonian syndrome that is indistinguishable from sporadic PD (Dauer and Przedborski, 2003). MPTP metabolite 1-methyl-4-pyridinium (MPP^+), an inhibitor of complex I of the mitochondrial respiration chain, is taken up by the terminals of dopaminergic neurons via the dopamine transporter (DAT), thereby causing the selective death of nigral neurons (Dauer and Przedborski, 2003). Although neuronal loss was not observed in L-hI93M mice at 20 weeks of age, we speculated that dopaminergic

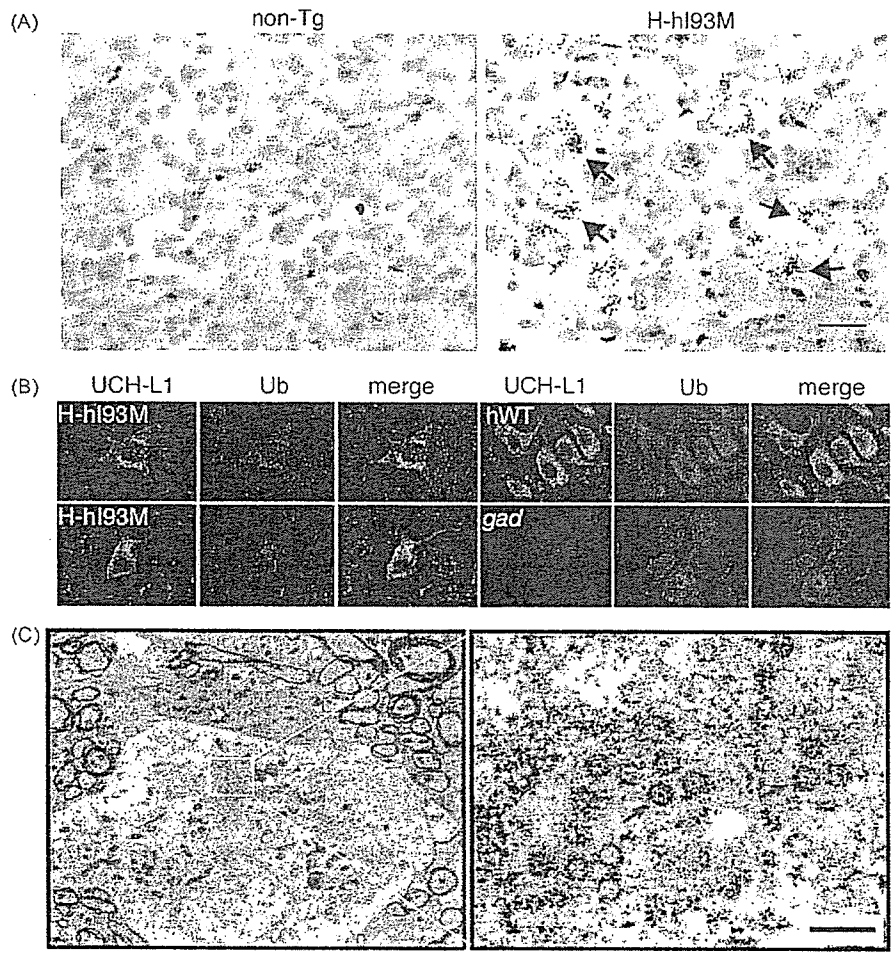

Fig. 4. Several neuropathological features reminiscent of PD are present in H-hI93M mice brains. (A) Silver staining of the substantia nigra at 12 weeks of age in non-Tg and H-hI93M mice. Note the presence of silver staining-positive argyrophilic grains in the cell bodies of some dopaminergic neurons in H-hI93M mice (arrows). This kind of abnormal structure was not seen in substantia nigra of non-Tg mice. Scale bar: 30 μm. (B) Confocal images of dopaminergic neurons from hWT, H-hI93M and *gad* mice. H-hI93M mice showed the formation of ubiquitin-positive cytoplasmic inclusions (red) co-localized with UCH-L1 staining (green) in the remaining nigral neurons at 20 weeks of age. Compared with the diffuse, reduced staining of ubiquitin in *gad* mice, nigral neurons from hWT mice also showed a diffuse pattern of staining but with fine small granular cytoplasmic staining (red) co-localized with UCH-L1 (green). (C) Electron micrographs of a nigral neuron from a 20-week-old H-hI93M mouse at the level of the cell body (left panel), and dense-core vesicles (red arrows) at higher magnification (right panel). Scale bar: 1 μm.

neurons of L-hI93M mice might be more susceptible to MPTP toxin compared to that of non-Tg mice or hWT mice. As expected, significantly fewer TH-positive neurons were observed in L-hI93M mice after MPTP treatment as compared with hWT or non-Tg control mice though hWT express higher *hUCHL1* compared to L-hI93M (Fig. 3C). The number of TH-positive neurons in MPTP-treated hWT mice was somewhat higher than that in non-Tg mice ($p < 0.001$). Taken together with the fact that expression of human UCH-L1 in L-hI93M is lower than that in hWT, these results suggest that the UCH-L1^{I93M} mutant, but not UCH-L1^{WT}, is specifically toxic to dopaminergic neurons.

3.3. Presence of neuropathology in dopaminergic neurons from H-hI93M mice

To evaluate the degenerative process of dopaminergic neurons, silver staining was used to indicate argyrophilic degenerating neurons (Lo Bianco et al., 2004). In non-Tg mice, no silver staining was observed, whereas scattered neurons containing grains that were silver staining positive were present in the substantia nigra of H-hI93M mice (Fig. 4A). The presence of intracellular inclusions called Lewy bodies and Lewy neurites are neuropathological characteristics of PD and are silver staining positive (Sandmann-Keil et al., 1999; Uchihara et al., 2005). It is also known that UCH-L1 and ubiquitin, as well as α-synuclein, are components of Lewy bodies (Lowe et al., 1990). Furthermore, UCH-L1 is tightly associated with mono-ubiquitin *in vivo* (Osaka et al., 2003). Thus, we expected that the silver staining-positive grains might have characteristic features of Lewy bodies. We therefore compared the immunohistochemical analysis of UCH-L1 and ubiquitin. Compared with reduced staining for ubiquitin in *gad* mice, strong and diffuse ubiquitin staining was observed in nigral neurons of hWT mice and non-Tg mice (data not shown), and this staining co-localized with UCH-L1, which is in agreement with our previous report (Osaka et al., 2003). In H-hI93M substantia nigra at 20 weeks of age, ubiquitin- and UCH-L1-positive cytoplasmic inclusions, a large aggregates with different morphology from small dots usually seen in hWT mice and non-Tg mice, were observed in a portion of the remaining nigral neurons (Fig. 4B). These inclusions were, however, α-synuclein or hematoxylin–eosin (HE) negative (data not shown). We could not observe UCH-L1- and ubiquitin-positive inclusions in L-hI93M mice (data not shown).

Another cellular characteristic of PD neuropathology is dense-core vesicles of about 80–200 nm in perikarya, which are frequently observed along with Lewy bodies in PD patients (Watanabe et al., 1977). We observed electron dense-core vesicles in the cytoplasm of ~30% of nigral neurons in H-hI93M mice using electron microscopy (Fig. 4C). In non-Tg mice, such vesicles with a similar shape were not detected in cell bodies but rather were seen in synaptic terminals. Taken together, our data indicate that degenerating dopaminergic neurons in the substantia nigra of H-hI93M mice are devoid of Lewy bodies but show some neuropathological features such as silver staining-positive argyrophilic grains, aggregates with UCH-L1 and ubiquitin, and dense-core vesicles in the perikarya.

3.4. Increased amount of SDS-insoluble but urea/SDS-soluble UCH-L1 in the midbrain of H-hI93M mice

UCH-L1^{I93M} has reduced α-helical content as compared with UCH-L1^{WT} (Nishikawa et al., 2003), and UCH-L1^{I93M} overexpression in COS7 cells results in more cells that contain cytoplasmic inclusions (Ardley et al., 2004). Thus, the presence of UCH-L1-positive inclusions in H-hI93M dopaminergic neurons led us to speculate whether UCH-L1^{I93M} would be less soluble than the wild-type protein *in vivo*. To biochemically characterize the changes in UCH-L1 deposited in the brains of H-hI93M mice, we sequentially extracted frozen midbrain tissues with 5% SDS (soluble fraction) and 8 M urea/5% SDS (insoluble fraction) and analyzed each fraction by immunoblotting with anti-UCH-L1. As expected, immunoblots of insoluble fractions showed a modest but statistically significant increase in UCH-L1 in the midbrains of H-hI93M mice as compared with those from a non-Tg mouse (Fig. 5A and B), indicating increased insolubility of UCH-L1^{I93M} *in vivo*, which might have resulted in dopaminergic neurotoxicity.

3.5. Decreased dopamine content in the striata of H-hI93M mice

Because the nigro-striatal pathway is severely affected in PD patients, and because our mice showed the degeneration of dopaminergic neurons in the substantia nigra, we evaluated the nerve terminals in the striatal pathway using

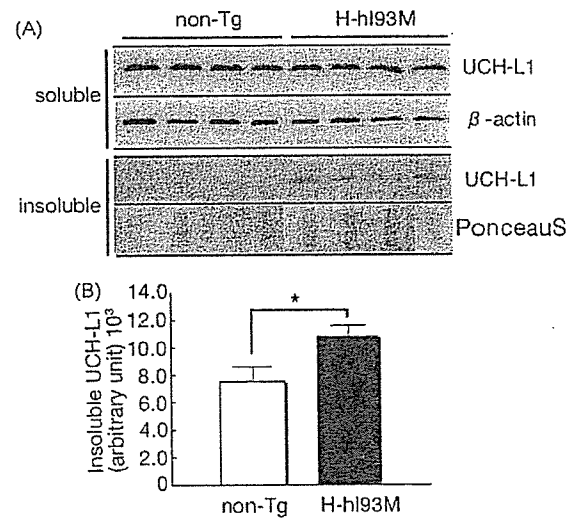

Fig. 5. Protein insolubility of UCH-L1 in H-hI93M Tg mice. (A) Immunoblotting analysis of UCH-L1 in soluble (5% SDS soluble) and insoluble (5% SDS insoluble and 8 M urea/5% SDS soluble) fractions from tissue containing the substantia nigra (11–13 weeks). Soluble fraction (5 μg for each) was probed with anti-UCH-L1 or anti-β-actin. Insoluble fraction (0.5 μg for each) was probed with anti-UCH-L1. One microgram of each insoluble fraction was applied to dot blotting and stained by Ponceau S to show that each fraction contained the same amount of total protein. A slight increase in the insolubility of UCH-L1 in the substantia nigra fraction from H-hI93M mice is seen as compared with that from non-Tg mice. (B) The experiment was done with H-hI93M mice and non-Tg littermates from five different litters, and the results of quantitative analyses in insoluble fraction is shown ($n = 5$ mice for each group).

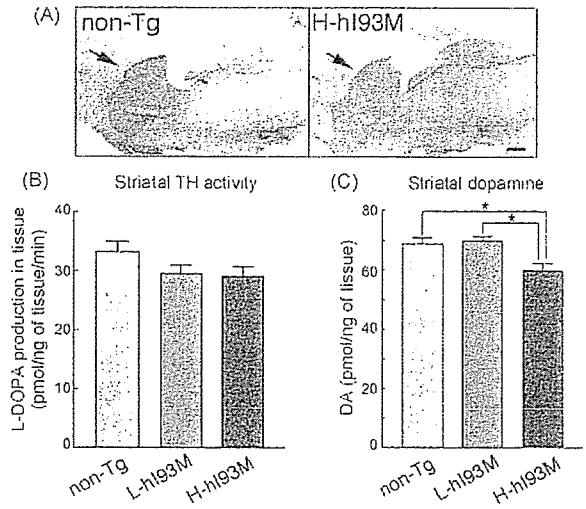

Fig. 6. H-hI93M mice show pathology in the striatum. Dopamine content and TH activity were lower in H-hI93M mice. (A) Sagittal sections from non-Tg and H-hI93M mice at 20 weeks of age were immunostained with the dopaminergic marker anti-TH. TH immunoreactivity is decreased in the nigro-striatal axons (arrows) of H-hI93M brains. Scale bar: 100 μm. (B) TH activity and (C) dopamine content were measured following extraction and homogenization of the mouse striatum of non-Tg, L-hI93M and H-hI93M mice at 20 weeks of age ($n = 4$; mean ± S.E). Significance was examined by a one-way ANOVA. $^{*}p < 0.05$.

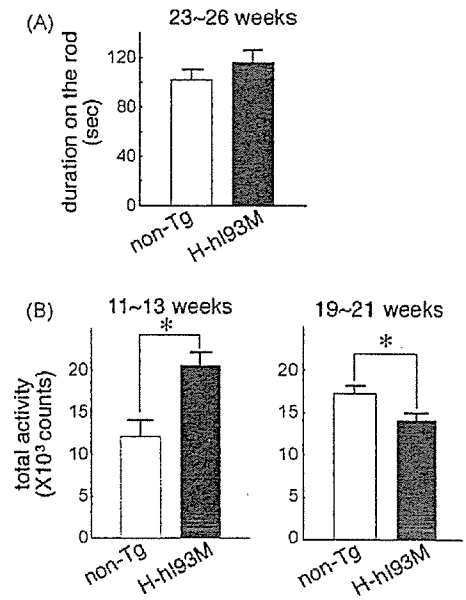

Fig. 7. H-hI93M transgenic mice show locomotor deficits. (A) Accelerated rota-rod analysis of H-hI93M and non-Tg mice ($n = 6$ for non-Tg and $n = 7$ for H-hI93M) at 23–26 weeks of age. Mice were placed on a rod, and their duration on the rod before falling off (mean value of three trials for each animal) was recorded. (B) Home cage monitor analysis of H-hI93M and non-Tg mice at 11–13 weeks of age (left; $n = 4$ for each line) and at 19–21 weeks of age (right; $n = 8$ for non-Tg and $n = 10$ for H-hI93M). Note the significant hypolocomotion of H-hI93M mice as compared with non-Tg mice at 19–21 weeks of age. Values are the mean ± S.E.M. Significance was examined using the unpaired Student's *t*-test. $^{*}p < 0.05$.

immunohistochemical and biochemical analyses. In agreement with the reduction of TH-positive dopaminergic neurons in the substantia nigra, nigro-striatal fibers in H-hI93M mice showed decreased immunoreactivity for TH as compared with that of non-Tg mice (Fig. 6A). TH activity, analyzed by determining L-DOPA production in the striatal tissues, also showed a tendency to decline in H-hI93M mice, although it was not significantly different (Fig. 6B). Loss of dopaminergic neurons in the substantia nigra and decreased TH activity in the striatum of H-hI93M mice prompted us to examine the concentration of striatal dopamine. Compared with non-Tg mice, H-hI93M mice showed a significant reduction of dopamine content in the striatum (Fig. 6C).

3.6. Decreased spontaneous, voluntary movements of H-hI93M mice

Given the prominent loss of dopaminergic neurons in the substantia nigra and the reduction in dopamine content in the striatum of H-hI93M mice, we next assessed the locomotor abilities of H-hI93M mice using a battery of well-established behavioral tests. Involuntary movement was analyzed by the rota-rod test (Goldberg et al., 2005) on 23–26-week-old mice. H-hI93M mice and non-Tg mice were similarly able to maintain their balance on the rotating rod during rod acceleration before falling off (Fig. 7A). We next analyzed spontaneous, voluntary movements with a locomotor activity test (Goldberg et al., 2005). Unexpectedly, 11–13-week-old H-hI93M mice showed significant hyperlocomotion during active periods (i.e., at night) as compared with non-Tg mice during home cage monitoring (Fig. 7B). However, 19–21-week-old H-hI93M mice showed a modest but significant reduction in locomotor activity during active periods as compared with non-Tg mice (Fig. 7B). These results indicate that, in addition to the neuropathological changes, H-hI93M mice exhibit mild behavioral deficits related to PD.

4. Discussion

In this study, we characterized transgenic mice expressing hUCH-L1^{I93M}, a mutation with presumptive association with familial PD, in the brain. Our previous attempt of making mouse UCH-L1^{WT} Tg mice under various higher expressing promoters, such as EF1α, resulted in an infertility of mice, thus it was impossible to maintain the lines. This failure resulted from the effect of overexpressing UCH-L1 in the testis/ovary leading to an increased apoptosis in these reproductive organs, although we did not find obvious morphological differences in the brain (Wang et al., 2006). Thus, we used *PDGF-B* promoter in this study to avoid massive expression of the transgene.

Two lines of hUCH-L1^{I93M} Tg mice and one line of hUCH-L1^{WT} Tg mice were viable and fertile without any predictable abnormalities. All of the three Tg lines expressed very limited levels of the human *UCHL1* gene with a maximum transcript ratio of about 1/100 as compared with the endogenous mouse *Uchl1*. However, immunohistological analysis indicated that higher level of hUCH-L1^{I93M} expression could be detected in the large number of neurons in the substantia nigra of

H-hI93M/gad mice at 2 weeks of age. In addition, there is a difference in the morphology of hUCH-L1^{I93M} expressing neurons, reminiscent of dying neurons, in the substantia nigra of H-hI93M/gad mice among 7 and 20 weeks of age. We also observed an eventual decline in the number of UCH-L1-positive neurons in H-hI93M/gad mice, as they age. Furthermore, the dopaminergic neurons in the substantia nigra of H-hI93M mice at 12 weeks of age showed silver staining-positive argylophilic grains, which represent neurons undergoing degeneration (Lo Bianco et al., 2004). Since we observed a loss of dopaminergic neurons in the substantia nigra and reduced dopamine content in the striatum of H-hI93M mice at 20 weeks of age, our results indicate the possibility that hUCH-L1^{I93M} expressing dopaminergic neurons degenerate with age.

In addition to cell loss, several neuropathological features were observed in the substantia nigra of H-hI93M mice. Dopaminergic neurons had (1) electron dense-core vesicles in the perikarya, and (2) cytoplasmic inclusions that were positive for both UCH-L1 and ubiquitin. Despite these features, we did not observe eosinophilic or α-synuclein-positive Lewy bodies at the substantia nigra in our morphological analyses. Thus, the mouse dopaminergic neurons expressing UCH-L1^{I93M} may die prior to the formation of Lewy bodies, or those mice might form these structures at stages beyond the period of our study.

The mechanisms responsible for dopaminergic cell loss in the substantia nigra of H-hI93M mice remain elusive. The I93M mutation in UCH-L1 reduces its hydrolase activity by about 50%, which has been suggested as a cause for the pathogenesis of PD (Nishikawa et al., 2003). However, we have not found clear evidence for nigro-striatal dopaminergic pathology in *gad* mice (data not shown). Since expression of UCH-L1 is not detected in gad mice, the reduction of hydrolase activity alone would not be the cause of PD. In light of our finding here that transgenic expression of UCH-L1^{I93M} results in dopaminergic pathology in mice, it would seem that this mutation elicits a gain of toxic function leading to the neuronal toxicity in the substantia nigra.

Our previous work using circular dichroism suggests that the I93M mutation reduces the α-helical content of UCH-L1 (Nishikawa et al., 2003). Recently, we had also showed, using small-angle neutron scattering, that wild-type or I93M mutant UCH-L1 exists as a dimmer in an aqueous solution. Moreover, their configuration differed; wild-type UCH-L1 has ellipsoidal shape where as I93M mutant has more globular shape (Naito et al., 2006). Cells expressing UCH-L1^{I93M} are more prone to form inclusions (Ardley et al., 2004). Proteomic analysis of autopsied brains from PD patients and AD patients shows that UCH-L1 is extensively modified by carbonyl formation, methionine oxidation and cysteine oxidation in the diseased brains (Choi et al., 2004). These modifications are shown to result from oxidative stress (Choi et al., 2004). We show here that I93M mutation in UCH-L1 increases its insolubility *in vivo*. From the very limited expression of human UCH-L1 I93M, it is possible to speculate that endogenous mouse UCH-L1 might become insoluble in the presence of I93M UCH-L1. In addition, L-hI93M neurons were more susceptible than hWT or non-Tg neurons to MPTP, an inhibitor of complex I. This observation suggests that UCH-L1^{I93M} easily gains toxicity under oxidative stress. The conformational change and/or the additional methionine oxidation in UCH-L1 caused by I93M mutation may cause increased insolubility and lead to the gain of a toxic function.

In addition, our behavioral analysis revealed that H-hI93M mice exhibit very slight defects in spontaneous, voluntary movement, as shown by their hyperlocomotion at 11–13 weeks of age and by their hypolocomotion at 19–21 weeks of age in the home cage monitor test. Patients with PD exhibit no clinical symptoms until 70–80% of dopaminergic neurons are lost (Dauer and Przedborski, 2003). Thus, the level of dopaminergic neuronal loss seen in H-hI93M mice might not be sufficient to produce severe clinical phenotypes. It is difficult to explain the hyperlocomotion detected at 11–13 weeks of age, by simple changes in the nigro-striatal pathway. Other brain areas might be related to the locomotor changes seen in H-hI93M mice. We will need further analysis to connect the dopaminergic cell loss and defects in spontaneous, voluntary movement in H-hI93M mice.

In attempts to replicate neuropathological aspects of PD, several of the familial PD genes have been altered in mice. Up to date, α-synuclein Tg mice with or without mutation (Fernagut and Chesselet, 2004), parkin knockout mice (Goldberg et al., 2003; Itier et al., 2003; Palacino et al., 2004; Perez and Palmiter, 2005; Von Coelln et al., 2004), and DJ-1 knockout mice (Chen et al., 2005; Goldberg et al., 2005; Kim et al., 2005) have been reported. Although these mice show some alterations in the function of dopaminergic neurons, none has dopaminergic neuron loss in the substantia nigra. Thus, we have developed the first mouse model with an alteration in a familial PD gene that leads to dopaminergic cell loss. Further analysis of these mice will help establish the role of UCH-L1 in PD, which may elucidate a common pathway for both familial and sporadic PD.

Acknowledgements

This work was supported by the Program for Promotion of Fundamental Studies in Health Sciences of the National Institute of Biomedical Innovation of Japan (KW); Grants-in-Aid for Scientific Research from the Ministry of Health, Labour and Welfare of Japan (KW); Grants-in-Aid for Scientific Research from the Ministry of Education, Culture, Sports, Science and Technology of Japan (KW); a grant from Japan Science and Technology Cooperation and a High Technology Research Center Grant (YM). We thank M. Shikama for the care and breeding of animals, H. Fujita for genotyping of animals, H. Kikuchi for technical assistance with tissue sections and N. Takagaki for the support in English. We also thank Dr. H. Hohjo for letting us use the home cage monitor.

References

Aoki, S., Su, Q., Li, H., Nishikawa, K., Ayukawa, K., Hara, Y., Namikawa, K., Kiryu-Seo, S., Kiyama, H., Wada, K., 2002. Identification of an axotomy-induced glycosylated protein, AIGP1, possibly involved in cell death triggered by endoplasmic reticulum-Golgi stress. J. Neurosci. 22, 10751–10760.

Ardley, H.C., Scott, G.B., Rose, S.A., Tan, N.G., Robinson, P.A., 2004. UCH-L1 aggresome formation in response to proteasome impairment indicates a role in inclusion formation in Parkinson's disease. J. Neurochem. 90, 379–391.

Bonifati, V., Rizzu, P., van Baren, M.J., Schaap, O., Breedveld, G.J., Krieger, E., Dekker, M.C., Squitieri, F., Ibanez, P., Joosse, M., van Dongen, J.W., Vanacore, N., van Swieten, J.C., Brice, A., Meco, G., van Duijn, C.M., Oostra, B.A., Heutink, P., 2003. Mutations in the DJ-1 gene associated with autosomal recessive early-onset parkinsonism. Science 299, 256–259.

Chartier-Harlin, M.C., Kachergus, J., Roumier, C., Mouroux, V., Douay, X., Lincoln, S., Levecque, C., Larvor, L., Andrieux, J., Hulihan, M., Waucquier, N., Defebvre, L., Amouyel, P., Farrer, M., Destee, A., 2004. Alpha-synuclein locus duplication as a cause of familial Parkinson's disease. Lancet 364, 1167–1169.

Chen, L., Cagniard, B., Mathews, T., Jones, S., Koh, H.C., Ding, Y., Carvey, P.M., Ling, Z., Kang, U.J., Zhuang, X., 2005. Age-dependent motor deficits and dopaminergic dysfunction in DJ-1 null mice. J. Biol. Chem. 280, 21418–21426.

Choi, J., Levey, A.I., Weintraub, S.T., Rees, H.D., Gearing, M., Chin, L.S., Li, L., 2004. Oxidative modifications and down-regulation of ubiquitin carboxyl-terminal hydrolase L1 associated with idiopathic Parkinson's and Alzheimer's diseases. J. Biol. Chem. 279, 13256–13264.

Dauer, W., Przedborski, S., 2003. Parkinson's disease: mechanisms and models. Neuron 39, 889–909.

Farrer, M., Kachergus, J., Forno, L., Lincoln, S., Wang, D.S., Hulihan, M., Maraganore, D., Gwinn-Hardy, K., Wszolek, Z., Dickson, D., Langston, J.W., 2004. Comparison of kindreds with parkinsonism and alpha-synuclein genomic multiplications. Ann. Neurol. 55, 174–179.

Fernagut, P.O., Chesselet, M.F., 2004. Alpha-synuclein and transgenic mouse models. Neurobiol. Dis. 17, 123–130.

Furuya, T., Hayakawa, H., Yamada, M., Yoshimi, K., Hisahara, S., Miura, M., Mizuno, Y., Mochizuki, H., 2004. Caspase-11 mediates inflammatory dopaminergic cell death in the 1-methyl-4-phenyl-1,2,3,6-tetrahydropyridine mouse model of Parkinson's disease. J. Neurosci. 24, 1865–1872.

Goldberg, M.S., Fleming, S.M., Palacino, J.J., Cepeda, C., Lam, H.A., Bhatnagar, A., Meloni, E.G., Wu, N., Ackerson, L.C., Klapstein, G.J., Gajendiran, M., Roth, B.L., Chesselet, M.F., Maidment, N.T., Levine, M.S., Shen, J., 2003. Parkin-deficient mice exhibit nigrostriatal deficits but not loss of dopaminergic neurons. J. Biol. Chem. 278, 43628–43635.

Goldberg, M.S., Pisani, A., Haburcak, M., Vortherms, T.A., Kitada, T., Costa, C., Tong, Y., Martella, G., Tscherter, A., Martins, A., Bernardi, G., Roth, B.L., Pothos, E.N., Calabresi, P., Shen, J., 2005. Nigrostriatal dopaminergic deficits and hypokinesia caused by inactivation of the familial Parkinsonism-linked gene DJ-1. Neuron 45, 489–496.

Hemelaar, J., Borodovsky, A., Kessler, B.M., Reverter, D., Cook, J., Kolli, N., Gan-Erdene, T., Wilkinson, K.D., Gill, G., Lima, C.D., Ploegh, H.L., Ovaa, H., 2004. Specific and covalent targeting of conjugating and deconjugating enzymes of ubiquitin-like proteins. Mol. Cell. Biol. 24, 84–95.

Hooper, D., Kawamura, M., Hoffman, B., Kopin, I.J., Hunyady, B., Mezey, E., Eisenhofer, G., 1997. Tyrosine hydroxylase assay for detection of low levels of enzyme activity in peripheral tissues. J. Chromatogr. B: Biomed. Sci. Appl. 694, 317–324.

Ibanez, P., Bonnet, A.M., Debarges, B., Lohmann, E., Tison, F., Pollak, P., Agid, Y., Durr, A., Brice, A., 2004. Causal relation between alpha-synuclein gene duplication and familial Parkinson's disease. Lancet 364, 1169–1171.

Itier, J.M., Ibanez, P., Mena, M.A., Abbas, N., Cohen-Salmon, C., Bohme, G.A., Laville, M., Pratt, J., Corti, O., Pradier, L., Ret, G., Joubert, C., Periquet, M., Araujo, F., Negroni, J., Casarejos, M.J., Canals, S., Solano, R., Serrano, A., Gallego, E., Sanchez, M., Denefle, P., Benavides, J., Tremp, G., Rooney, T.A., Brice, A., Garcia de Yebenes, J., 2003. Parkin gene inactivation alters behaviour and dopamine neurotransmission in the mouse. Hum. Mol. Genet. 12, 2277–2291.

Kahle, P.J., Neumann, M., Ozmen, L., Muller, V., Odoy, S., Okamoto, N., Jacobsen, H., Iwatsubo, T., Trojanowski, J.Q., Takahashi, H., Wakabayashi, K., Bogdanovic, N., Riederer, P., Kretzschmar, H.A., Haass, C., 2001. Selective insolubility of alpha-synuclein in human Lewy body diseases is recapitulated in a transgenic mouse model. Am. J. Pathol. 159, 2215–2225.

Kim, R.H., Smith, P.D., Aleyasin, H., Hayley, S., Mount, M.P., Pownall, S., Wakeham, A., You-Ten, A.J., Kalia, S.K., Horne, P., Westaway, D., Lozano, A.M., Anisman, H., Park, D.S., Mak, T.W., 2005. Hypersensitivity of DJ-1-deficient mice to 1-methyl-4-phenyl-1,2,3,6-tetrahydropyrindine (MPTP) and oxidative stress. Proc. Natl. Acad. Sci. U.S.A. 102, 5215–5220.

Kitada, T., Asakawa, S., Hattori, N., Matsumine, H., Yamamura, Y., Minoshima, S., Yokochi, M., Mizuno, Y., Shimizu, N., 1998. Mutations in the parkin gene cause autosomal recessive juvenile parkinsonism. Nature 392, 605–608.

Kruger, R., Kuhn, W., Muller, T., Woitalla, D., Graeber, M., Kosel, S., Przuntek, H., Epplen, J.T., Schols, L., Riess, O., 1998. Ala30Pro mutation in the gene encoding alpha-synuclein in Parkinson's disease. Nat. Genet. 18, 106–108.

Larsen, C.N., Krantz, B.A., Wilkinson, K.D., 1998. Substrate specificity of deubiquitinating enzymes: ubiquitin C-terminal hydrolases. Biochemistry 37, 3358–3368.

Leroy, E., Boyer, R., Auburger, G., Leube, B., Ulm, G., Mezey, E., Harta, G., Brownstein, M.J., Jonnalagada, S., Chernova, T., Dehejia, A., Lavedan, C., Gasser, T., Steinbach, P.J., Wilkinson, K.D., Polymeropoulos, M.H., 1998. The ubiquitin pathway in Parkinson's disease. Nature 395, 451–452.

Lincoln, S., Vaughan, J., Wood, N., Baker, M., Adamson, J., Gwinn-Hardy, K., Lynch, T., Hardy, J., Farrer, M., 1999. Low frequency of pathogenic mutations in the ubiquitin carboxy-terminal hydrolase gene in familial Parkinson's disease. Neuroreport 10, 427–429.

Liu, Y., Fallon, L., Lashuel, H.A., Liu, Z., Lansbury Jr., P.T., 2002. The UCH-L1 gene encodes two opposing enzymatic activities that affect alpha-synuclein degradation and Parkinson's disease susceptibility. Cell 111, 209–218.

Lo Bianco, C., Schneider, B.L., Bauer, M., Sajadi, A., Brice, A., Iwatsubo, T., Aebischer, P., 2004. Lentiviral vector delivery of parkin prevents dopaminergic degeneration in an alpha-synuclein rat model of Parkinson's disease. Proc. Natl. Acad. Sci. U.S.A. 101, 17510–17515.

Lowe, J., McDermott, H., Landon, M., Mayer, R.J., Wilkinson, K.D., 1990. Ubiquitin carboxyl-terminal hydrolase (PGP 9.5) is selectively present in ubiquitinated inclusion bodies characteristic of human neurodegenerative diseases. J. Pathol. 161, 153–160.

Maraganore, D.M., Farrer, M.J., Hardy, J.A., Lincoln, S.J., McDonnell, S.K., Rocca, W.A., 1999. Case-control study of the ubiquitin carboxy-terminal hydrolase L1 gene in Parkinson's disease. Neurology 53, 1858–1860.

Mochizuki, H., Hayakawa, H., Migita, M., Shibata, M., Tanaka, R., Suzuki, A., Shimo-Nakanishi, Y., Urabe, T., Yamada, M., Tamayose, K., Shimada, T., Miura, M., Mizuno, Y., 2001. An AAV-derived Apaf-1 dominant negative inhibitor prevents MPTP toxicity as antiapoptotic gene therapy for Parkinson's disease. Proc. Natl. Acad. Sci. U.S.A. 98, 10918–10923.

Naito, S., Mochizuki, H., Yasuda, T., Mizuno, Y., Furusaka, M., Ikeda, S., Adachi, T., Shimizu, H.M., Suzuki, J., Fujiwara, S., Okada, T., Nishikawa, K., Aoki, S., Wada, K., 2006. Characterization of multimetric variants of ubiquitin carboxyl-terminal hydrolase L1 in water by small-angle neutron scattering. Biochem. Biophys. Res. Commun. 339, 717–725.

Naoi, M., Takahashi, T., Nagatsu, T., 1988. Simple assay procedure for tyrosine hydroxylase activity by high-performance liquid chromatography employing coulometric detection with minimal sample preparation. J. Chromatogr. 427, 229–238.

Nishikawa, K., Li, H., Kawamura, R., Osaka, H., Wang, Y.L., Hara, Y., Hirokawa, T., Manago, Y., Amano, T., Noda, M., Aoki, S., Wada, K., 2003. Alterations of structure and hydrolase activity of parkinsonism-associated human ubiquitin carboxyl-terminal hydrolase L1 variants. Biochem. Biophys. Res. Commun. 304, 176–183.

Osaka, H., Wang, Y.L., Takada, K., Takizawa, S., Setsuie, R., Li, H., Sato, Y., Nishikawa, K., Sun, Y.J., Sakurai, M., Harada, T., Hara, Y., Kimura, I., Chiba, S., Namikawa, K., Kiyama, H., Noda, M., Aoki, S., Wada, K., 2003. Ubiquitin carboxy-terminal hydrolase L1 binds to and stabilizes monoubiquitin in neuron. Hum. Mol. Genet. 12, 1945–1958.

Paisan-Ruiz, C., Jain, S., Evans, E.W., Gilks, W.P., Simon, J., van der Brug, M., Lopez de Munain, A., Aparicio, S., Gil, A.M., Khan, N., Johnson, J., Martinez, J.R., Nicholl, D., Carrera, I.M., Pena, A.S., de Silva, R., Lees, A., Marti-Masso, J.F., Perez-Tur, J., Wood, N.W., Singleton, A.B., 2004. Cloning of the gene containing mutations that cause PARK8-linked Parkinson's disease. Neuron 44, 595–600.

Palacino, J.J., Sagi, D., Goldberg, M.S., Krauss, S., Motz, C., Wacker, M., Klose, J., Shen, J., 2004. Mitochondrial dysfunction and oxidative damage in parkin-deficient mice. J. Biol. Chem. 279, 18614–18622.

Perez, F.A., Palmiter, R.D., 2005. Parkin-deficient mice are not a robust model of parkinsonism. Proc. Natl. Acad. Sci. U.S.A. 102, 2174–2179.

Polymeropoulos, M.H., Lavedan, C., Leroy, E., Ide, S.E., Dehejia, A., Dutra, A., Pike, B., Root, H., Rubenstein, J., Boyer, R., Stenroos, E.S., Chandrasekharappa, S., Athanassiadou, A., Papapetropoulos, T., Johnson, W.G., Lazzarini, A.M., Duvoisin, R.C., Di Iorio, G., Golbe, L.I., Nussbaum, R.L., 1997. Mutation in the alpha-synuclein gene identified in families with Parkinson's disease. Science 276, 2045–2047.

Rane, N.S., Yonkovich, J.L., Hegde, R.S., 2004. Protection from cytosolic prion protein toxicity by modulation of protein translocation. EMBO J. 23, 4550–4559.

Saigoh, K., Wang, Y.L., Suh. J.G., Yamanishi, T., Sakai, Y., Kiyosawa, H., Harada, T., Ichihara, N., Wakana, S., Kikuchi, T., Wada, K., 1999. Intragenic deletion in the gene encoding ubiquitin carboxy-terminal hydrolase in gad mice. Nat. Genet. 23, 47–51.

Sandmann-Keil, D., Braak, H., Okochi, M., Haass, C., Braak, E., 1999. Alpha-synuclein immunoreactive Lewy bodies and Lewy neurites in Parkinson's disease are detectable by an advanced silver-staining technique. Acta Neuropathol. (Berl.) 98, 461–464.

Sasahara, M., Fries, J.W., Raines, E.W., Gown, A.M., Westrum, L.E., Frosch, M.P., Bonthron, D.T., Ross, R., Collins, T., 1991. PDGF B-chain in neurons of the central nervous system, posterior pituitary, and in a transgenic model. Cell 64, 217–227.

Singleton, A.B., Farrer, M., Johnson, J., Singleton, A., Hague, S., Kachergus, J., Hulihan, M., Peuralinna, T., Dutra, A., Nussbaum, R., Lincoln, S., Crawley, A., Hanson, M., Maraganore, D., Adler, C., Cookson, M.R., Muenter, M., Baptista, M., Miller, D., Blancato, J., Hardy, J., Gwinn-Hardy, K., 2003. Alpha-synuclein locus triplication causes Parkinson's disease. Science 302, 841.

Uchihara, T., Nakamura, A., Mochizuki, Y., Hayashi, M., Orimo, S., Isozaki, E., Mizutani, T., 2005. Silver stainings distinguish Lewy bodies and glial cytoplasmic inclusions: comparison between Gallyas-Braak and Campbell-Switzer methods. Acta Neuropathol. (Berl.) 110, 255–260.

Valente, E.M., Abou-Sleiman, P.M., Caputo, V., Muqit, M.M., Harvey, K., Gispert, S., Ali, Z., Del Turco, D., Bentivoglio, A.R., Healy, D.G., Albanese, A., Nussbaum, R., Gonzalez-Maldonado, R., Deller, T., Salvi, S., Cortelli, P., Gilks, W.P., Latchman, D.S., Harvey, R.J., Dallapiccola, B., Auburger, G., Wood, N.W., 2004. Hereditary early-onset Parkinson's disease caused by mutations in PINK1. Science 304, 1158–1160.

Vila, M., Przedborski, S., 2004. Genetic clues to the pathogenesis of Parkinson's disease. Nat. Med. 10 (Suppl.), S58–S62.

Von Coelln, R., Thomas, B., Savitt, J.M., Lim, K.L., Sasaki, M., Hess, E.J., Dawson, V.L., Dawson, T.M., 2004. Loss of locus coeruleus neurons and reduced startle in parkin null mice. Proc. Natl. Acad. Sci. U.S.A. 101, 10744–10749.

Wang, Y.L., Liu, W., Sun, Y.J., Kwon, J., Setsuie, R., Osaka, H., Noda, M., Aoki, S., Yoshikawa, Y., Wada, K., 2006. Overexpression of ubiquitin carboxyl-terminal hydrolase L1 arrests spermatogenesis in transgenic mice. Mol. Reprod. Develop. 73, 40–49.

Wang, Y.L., Takeda, A., Osaka, H., Hara, Y., Furuta, A., Setsuie, R., Sun, Y.J., Kwon, J., Sato, Y., Sakurai, M., Noda, M., Yoshikawa, Y., Wada, K., 2004. Accumulation of beta- and gamma-synucleins in the ubiquitin carboxyl-terminal hydrolase L1-deficient gad mouse. Brain Res. 1019, 1–9.

Watanabe, I., Vachal, E., Tomita, T., 1977. Dense core vesicles around the Lewy body in incidental Parkinson's disease: an electron microscopic study. Acta Neuropathol. (Berl.) 39, 173–175.

Wilkinson, K.D., Lee, K.M., Deshpande, S., Duerksen-Hughes, P., Boss, J.M., Pohl, J., 1989. The neuron-specific protein PGP 9.5 is a ubiquitin carboxyl-terminal hydrolase. Science 246, 670–673.

Zimprich, A., Biskup, S., Leitner, P., Lichtner, P., Farrer, M., Lincoln, S., Kachergus, J., Hulihan, M., Uitti, R.J., Calne, D.B., Stoessl, A.J., Pfeiffer, R.F., Patenge, N., Carbajal, I.C., Vieregge, P., Asmus, F., Muller-Minsk, B., Dickson, D.W., Meeting, T., Strom, T.M., Wszolek. Z.K., Gasser, T., 2004. Mutations in LRRK2 cause autosomal-dominant parkinsonism with allomorphic pathology. Neurone 44, 601–607.

Available online at www.sciencedirect.com
SCIENCE DIRECT®
European Journal of Pharmacology 536 (2006) 62–68
ELSEVIER
ejp
www.elsevier.com/locate/ejphar

Identification of a novel regulatory mechanism for norepinephrine transporter activity by the IP_3 receptor

Taiju Amano [a,b], Shunsuke Aoki [b,c,d,*], Rieko Setsuie [a,b], Mikako Sakurai [a,b], Keiji Wada [b], Mami Noda [a]

[a] Laboratory of Pathophysiology, Graduate School of Pharmaceutical Sciences, Kyushu University, Fukuoka 812-8582, Japan
[b] Department of Degenerative Neurological Diseases, National Institute of Neuroscience, NCNP, Tokyo 187-8502, Japan
[c] Department of Demyelinating Disease and Aging, National Institute of Neuroscience, NCNP, Tokyo 187-8502, Japan
[d] New Energy and Industrial Technology Development Organization (NEDO), Kawasaki, Kanagawa 212-8554, Japan

Received 17 October 2005; received in revised form 27 January 2006; accepted 21 February 2006
Available online 28 February 2006

Abstract

The norepinephrine transporter (NET) plays a crucial role in noradrenergic neurotransmission and is a target of many antidepressants and psychostimulants. Intracellular Ca^{2+} is reportedly involved in regulating NET activity, but the detailed mechanism is not clear. We employed a norepinephrine uptake assay using SH-SY5Y cells and found that the IP_3 receptor inhibitors, 2-aminoethoxydiphenyl borate and xestospongin C, reduced the NET V_{max}. These reductions were accompanied by the decreased cell surface expression of NET. Our findings suggest that intracellular Ca^{2+} mobilized by IP_3 receptor is required for the maintenance of NET activity. This adds another pathway involving Ca^{2+} for the regulation of NET to other known mechanisms providing intracellular Ca^{2+}.

Keywords: Norepinephrine; Transporter; Calcium; Membrane traffic

1. Introduction

Norepinephrine is an important neurotransmitter that controls alertness, attention, mood, and learning/memory in the central nervous system (Foote et al., 1983). It was suggested that noradrenergic neuron dysfunctions may cause many disorders, such as depression (Brunello et al., 2002), attention deficit hyperactivity disorder (ADHD) (Biederman and Spencer, 1999) and posttraumatic stress disorder (PTSD) (Hageman et al., 2001). Indeed, alterations of regional norepinephrine function may underlie these norepinephrine-related disorders (Tanaka, 1999; Thomas et al., 1994). Noradrenergic neurons are localized in brain stem nuclei A1-7 and project extensively to the cortex, amygdala, hypothalamus, hippocampus and septum (Foote et al., 1983). Norepinephrine is released at the terminals within each brain region, and it has been reported that norepinephrine concentration at each target is regulated in a region-specific manner. For example, regional variations of norepinephrine concentration are observed in the noradrenergic terminals of different cortical regions such as the prefrontal, somatosensory, and visual cortex (Brown et al., 1979; Levitt et al., 1984). However, the mechanisms that establish variations in norepinephrine concentration at each terminal are not clear. The norepinephrine transporter (NET) regulates norepinephrine concentration (Xu et al., 2000a). NET is a 12-transmembrane, Na^+/Cl^--dependent neurotransmitter transporter with cytoplasmic N and C termini (Pacholczyk et al., 1991). The characteristics of NET are shared with the glycine transporter (GLYT), dopamine transporter (DAT) and serotonin transporter (SERT). NET is a target of tricyclic antidepressants and psychostimulants. Dysfunction of NET induces abnormal extracellular neurotransmitter concentrations at the prefrontal

* Corresponding author. Department of Degenerative Neurological Diseases, Department of Demyelinating Disease and Aging, National Institute of Neuroscience, NCNP, New Energy and Industrial Technology Development Organization (NEDO), 4-1-1, Ogawahigashi, Kodaira, Tokyo 187-8502, Japan. Tel.: +81 42 346 1715; fax: +81 42 346 1745.
E-mail address: aokis@ncnp.go.jp (S. Aoki).

0014-2999/$ - see front matter © 2006 Elsevier B.V. All rights reserved.
doi:10.1016/j.ejphar.2006.02.041

cortex, hippocampus and cerebellum (Xu et al., 2000a). On the other hand, NET activity in SH-SY5Y cells is regulated by intracellular signaling factors such as protein kinase C (PKC) (Apparsundaram et al., 1998b) and protein phosphatase 2A (PP2A) (Bauman et al., 2000), which modulate the cell surface NET. However, the molecular mechanism of NET regulation at each terminal site of noradrenergic neurons is not clear.

NET activity is reduced in the presence of the membrane-permeable Ca^{2+} chelator, 1,2-bis (o-aminophenoxy) ethane-*N*, *N*,*N*′,*N*′-tetraacetic acid tetra (acetoxy-methyl) ester (BAPTA-AM) (Apparsundaram et al., 2001). Although PKC is Ca^{2+}-dependent, its activation reduces NET activity (Apparsundaram et al., 1998b), suggesting that another Ca^{2+}-dependent factor may potentiate NET activity. Activation of PKC requires both Ca^{2+} and diacylglycerol. Both diacylglycerol and inositol 1,4,5-trisphosphate (IP_3) are products of the breakdown of phosphatidylinositol 4,5-bisphosphate by phospholipase C (PLC). IP_3 is a major inducer of intracellular Ca^{2+} release. Since intracellular Ca^{2+} signaling is strictly regulated to affect on site-specific signaling (i.e., via Ca^{2+} microdomains) (Becherer et al., 2003; Delmas et al., 2002; Olivos Ore and Artalejo, 2004; Zheng, 2000), the IP_3 receptor may be critical for regional regulation of NET at each noradrenergic terminal.

Here, we examined whether intracellular Ca^{2+} mediated by IP_3 receptor affects NET activity in the SH-SY5Y cells, which are human neuroblastoma cell lines expressing native NET. We found that the IP_3 receptor–Ca^{2+} pathway plays a critical role for the maintenance of NET activity. Our findings suggest that IP_3 receptor acts as a link between Ca^{2+} microdomains and NET regulation to modulate norepinephrine concentration.

2. Materials and methods

2.1. Cell culture

SH-SY5Y cells were obtained from American Type Culture Collection (ATCC, Manassas, VA) and maintained in Dulbecco's modified Eagle medium (DMEM) containing 10% fetal bovine serum (FBS), 4 mM L-glutamine, 100 U/ml penicillin, and 100 U/ml streptomycin in 5% CO_2 at 37 °C and plated in Falcon 100-mm dishes (Becton Dickinson, Franklin Lakes, NJ). Only three specific passages were used for the assay.

2.2. Materials

Reagents used to modify receptors and second messengers were obtained from the following sources: 2-aminoethoxydiphenyl borate (2APB), (Calbiochem, San Diego, CA); protease inhibitor cocktail (Roche, Mannheim, Germany); xestospongin C and $LaCl_3$ (Wako, Osaka, Japan); norepinephrine (= arterenol), ryanodine, cyclopiazonic acid (CPA), desipramine, BAPTA, BAPTA-AM and DMEM (Sigma, St. Louis, MO); [^{3}H] norepinephrine (L-[7,8-^{3}H] noradrenaline), (Amersham Biosciences Corp., Piscataway, NJ); 2-[4-(2-hydroxyethyl)-1-piperazinyl] ethanesulfonic acid (HEPES) and Calcium Kit-Fluo 3 (Dojindo, Tokyo, Japan); West Dura Extended Duration Substrate, horseradish peroxidase (HRP)-conjugated anti-mouse and anti-rabbit IgG, monomeric avidin beads and EZ-Link sulfo-NHS-LC-Biotin (Pierce, Rockford, IL); antibody against hNET (NET 1-17, Mab technology, Stone Mountain, GA); antibody against calnexin (Stressgen, Victoria, Canada). Other reagents were of analytical purity and were obtained from standard sources.

2.3. Norepinephrine uptake assay

NET activity was assessed as the uptake of [^{3}H] norepinephrine (velocity per total protein). The cells were collected by trypsinization, plated at 5×10^4 cells/well in collagen-coated 96-well dishes 24 h before experiments. For norepinephrine uptake studies, the culture medium was removed from 96-well plates, and the cells in each well were washed with Krebs–Ringer–HEPES (KRH) buffer (125 mM NaCl, 4.8 mM KCl, 1.3 mM $CaCl_2$, 1.2 mM $MgSO_4$, 1.2 mM KH_2PO_4, 5.6 mM glucose, 25 mM HEPES, 100 μM ascorbic acid, 50 μM pargyline, pH 7.4) at room temperature. To analyze NET kinetics, an norepinephrine uptake assay was performed using [^{3}H] norepinephrine and non-radiolabeled norepinephrine to obtain final concentrations of 0.2–7 μM. In other norepinephrine uptake analyses, cells were treated with each reagent for the signal transduction factor prior to the addition of 500 nM [^{3}H] norepinephrine. Cells were incubated at 37 °C for 10 min, and the assay was terminated by three rapid washes with ice-cold KRH buffer. The cells were then lysed in 0.1 N NaOH, and the lysate was applied to a Luma plate (Perkin Elmer, Wellesley, MA) and dried. The radioactivity was quantified using a Microbeta counter (Perkin Elmer). Nonspecific [^{3}H] norepinephrine uptake was determined using 1 μM desipramine and was subtracted from the total uptake to yield NET-specific uptake. An aliquot of extract was used to determine protein concentration using the Bio-Rad Protein Assay. Nonlinear curve fits of saturation data were calculated using the Eadie–Hofstee model, $V_o = -K_m \times V_o/S + V_{max}$. All the reagents used in our experiments affected the lactic acid dehydrogenase (LDH) assay for cytotoxicity by less than 5%.

2.4. Intracellular Ca^{2+} measurements

Intracellular Ca^{2+} was measured using the Calcium Kit-Fluo 3 (Dojindo). Briefly, 5×10^4 cells were incubated with Fluo-3 AM for 90 min and then placed in Ca^{2+}-free KRH buffer containing 0.1% dimethyl sulfoxide (DMSO; control) or one of the IP_3 receptor inhibitors, 20 μM 2APB or 10 μM xestospongin C. After 10 min, carbachol was added to yield a final concentration of 10 μM to initiate intracellular Ca^{2+} release. Fluorescence was monitored in a 1420 Multilabel counter (Perkin-Elmer, Turk, Finland) at 485 nm (excitation) and 530 nm (emission). Fluorescence data were acquired at a frame interval of 0.5 s.

2.5. Cell surface biotinylation

SH-SY5Y cells were plated at 5×10^6 cells into collagen or poly-L-ornithine coated 60-mm dish (Falcon) for 24 h. After

treatment with reagents for 15 min, norepinephrine (500 nM) was added and incubated for 10 min in KRH buffer. Next, cells were washed with ice-cold phosphate buffered saline/Ca^{2+}/Mg^{2+} (PBS/Ca^{2+}/Mg^{2+}; 138 mM NaCl, 2.7 mM KCl, 1.5 mM KH_2PO_4, 9.6 mM Na_2HPO_4, 1 mM $MgCl_2$, 0.1 mM $CaCl_2$, pH 7.3) and then treated with EZ-Link Sulfo-NHS-LC-Biotin (1.5 mg/ml, Pierce) at 4 °C for 1 h in PBS/Ca^{2+}/Mg^{2+}. The biotinylating reagents were removed and washed twice with 100 mM glycine in PBS/Ca^{2+}/Mg^{2+}. The biotinylation reaction was quenched by incubation in 100 mM glycine in PBS/Ca^{2+}/Mg^{2+} at 4 °C for 30 min, and washed three times with PBS/Ca^{2+}/Mg^{2+}. Cells in each dish or well were solubilized by Radioimmunoprecipitation Assay (RIPA) buffer (20 mM Tris pH 7.5, 137 mM NaCl, 1 mM EDTA, 0.1% sodium dodecyl sulfate (SDS), 1% Triton X-100, 1% sodium deoxycholate) containing protease inhibitor cocktail (Roch) and shaken at 4 °C for 1 h. Extracts were centrifuged at 20,000 ×*g* at 4 °C for 30 min. Aliquots of supernatants (total lysate) were removed and preserved in other tubes. Monomeric avidin beads (Pierce) that were washed in RIPA buffer were added to the remainder of the samples and shaken for 1 h at room temperature. The unbound fractions (non-biotinylated lysate) were removed by centrifugation and preserved in other tubes. The beads were washed three times with RIPA buffer and the absorbed proteins were eluted by Laemmli loading buffer (62.5 mM Tris–HCl, pH 6.8, 20% glycerol, 2% SDS, 5% β-mercaptoethanol and 0.1% bromophenol blue) with shaking for 30 min at room temperature. Total lysates and non-biotinylated lysates were diluted with 2× Laemmli loading buffer. All samples were resolved by 10% SDS-polyacrylamide gel electrophoresis (SDS-PAGE), prior to transfer to a polyvinylidene difluoride (PVDF) membrane (Bio-Rad, Hercules, CA). After blocking with 5% nonfat dried milk in PBS containing 0.1% Tween 20 (PBST), blots were probed with primary antibody. Following washes with PBST, proteins reacting with HRP-conjugated anti-mouse or rabbit IgG (secondary antibody, 1:20,000, Pierce) were visualized using SuperSignal West Dura Extended Duration Substrate (Pierce). Values of NET in total, non-biotinylated (intracellular) fraction, and the biotinylated (cell surface) fraction were normalized by the levels of calnexin immunoreactivity in total fraction.

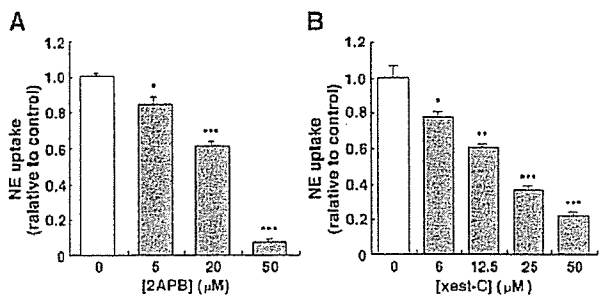

Fig. 1. The IP_3 receptor inhibitors 2APB and xestospongin C decreased NET activity. (A, B) Cells were incubated with vehicle or each reagent (37 °C, 15 min) followed by incubation with [^{3}H] norepinephrine (500 nM). The nonspecific signal was defined using 1 μM desipramine. Data represent means ±S.E.M. (n=3; *P<0.05, **P<0.01, ***P<0.001, vs. controls, ANOVA followed by the Dunnet's method).

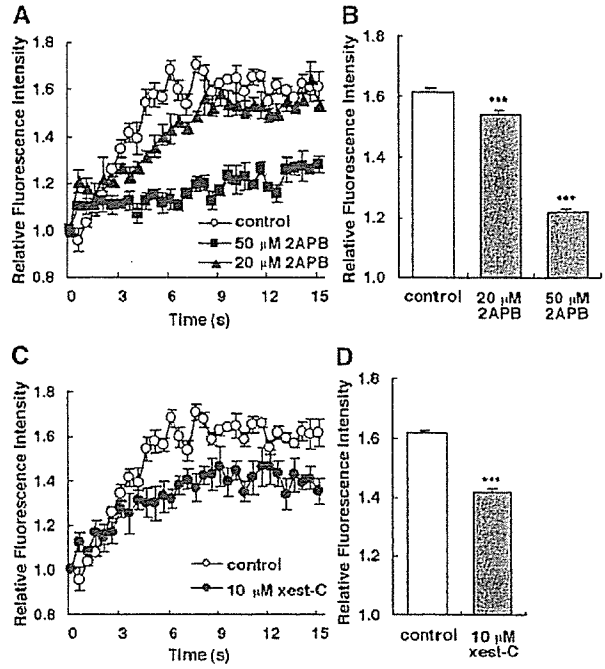

Fig. 2. The IP_3 receptor inhibitors 2APB and xestospongin C blocked the elevation of intracellular Ca^{2+} concentration. (A–D) Intracellular Ca^{2+} was monitored using the Ca^{2+}-sensitive fluorescent indicator, Fluo-3 AM. Cells were incubated with Fluo-3 AM for 90 min and then incubated in Ca^{2+}-free KRH buffer (compensated with 10 mM $MgCl_2$) containing 0.1% DMSO (control) or 20 μM/50 μM 2APB (A) or 10 μM xestospongin C (C), also in 0.1% DMSO. After 10 min, 10 μM (final concentration) carbachol was added to initiate intracellular Ca^{2+} release. The effects of 2APB and xestospongin C on intracellular Ca^{2+} release are presented as means of relative fluorescence intensity after the plateau (8–15 s, B, D). Data represent means±S.E.M. (n=3; ***P<0.001, vs. controls, ANOVA followed by the Dunnet's method (B) and Student's t test (D)).

2.6. Data analyses

Statistical analyses were performed by comparing mean values or mean percentages derived from each experiment. The Student's t test was used for statistical analysis of data involving comparisons between two groups. One-way analysis of variance (ANOVA) followed by the Bonferroni method was used for deducing statistical differences in experiments involving multiple comparisons. The Dunnet's test was used for comparison of a single control group to all other groups. All analyses were performed using PRISM version 3.0 (GraphPad Software, Inc., San Diego, CA).

3. Results

3.1. Effects of IP_3 receptor inhibitors on NET activity and intracellular Ca^{2+} concentration

To establish whether IP_3 receptor is involved in regulating NET activity, we examined the effect of two structurally different IP_3 receptor inhibitors, 2-aminoethoxydiphenyl borate (2APB) and xestospongin C, on NET activity in the human neuroblastoma cells, SH-SY5Y. Treatment with both IP_3

receptor inhibitors produced the reduction of NET activity (Fig. 1A, B).

Next, we tested whether IP_3 receptor inhibitors block the elevation of intracellular Ca^{2+} concentration induced by IP_3 receptor stimulation under our experimental condition. SH-SY5Y cells are reported to express muscarinic receptors (Kukkonen et al., 2001). Carbachol, a specific agonist for the muscarinic receptor, induced intracellular Ca^{2+} elevation via IP_3 generation (Kukkonen et al., 2001; Xu et al., 2000b). Thus we measured carbachol-stimulated Ca^{2+} elevation in SH-SY5Y cells with the fluorescent Ca^{2+} indicator, Fluo-3. As shown in Fig. 2A–D, the treatment of IP_3 receptor inhibitors significantly reduced intracellular Ca^{2+} elevation under extracellular Ca^{2+}-free condition (0–50 μM 2APB, 0–10 μM xestospongin C). Kukkonen et al. (2001) reported that 2APB failed to reduce the intracellular Ca^{2+} elevation in SH-SY5Y cells stimulated by carbachol under their experimental conditions. Although our data differed from the report, this discrepancy may be caused by the different 2APB incubation period or the extracellular Ca^{2+} concentration. Taken together, these results indicated that the elevation of intracellular Ca^{2+} concentration mediated by IP_3 receptor links with NET activity.

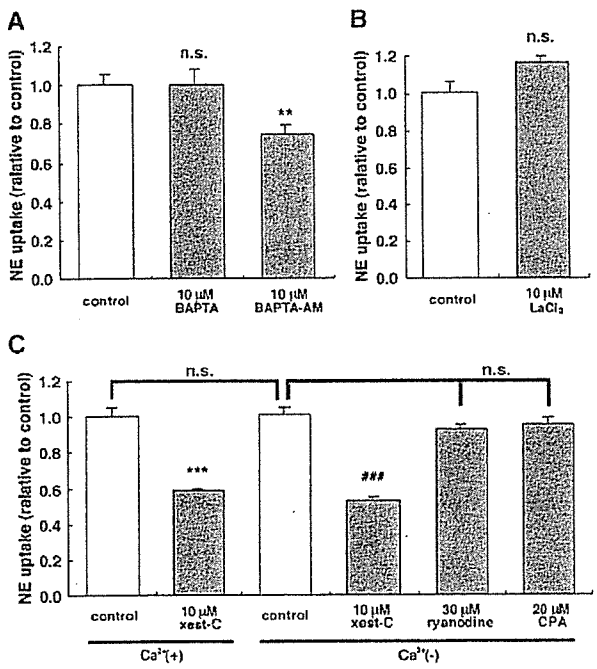

Fig. 3. Effects of intracellular and extracellular Ca^{2+} on NET activity. (A) Effect of the membrane-permeable Ca^{2+} chelator BAPTA-AM, and the non-membrane permeable chelator, BAPTA, on NET activity. Cells were incubated with 10 μM BAPTA or 10 μM BAPTA-AM in KRH buffer containing 0.1% bovine serum albumin (BSA) for 2 h and then assayed for NET activity. The nonspecific signal was defined using 1 μM desipramine. Data represent means±S.E.M. (n=3, n.s., not significant, $^{**}P<0.01$, ANOVA followed by the Bonferroni method). (B) Effect of the SOC channel inhibitor, $LaCl_3$ on NET activity. Cells were incubated with 10 μM $LaCl_3$ for 15 min and then assayed for NET activity. Data represent means±S.E.M. (n=3, n.s., not significant, Student's t test). (C) Effect of extracellular Ca^{2+}, ryanodine receptor and xestospongin C (xest-C) on NET activity. Cells were treated with the IP_3 receptor inhibitor, 10 μM xestospongin C, the ryanodine receptor agonist, ryanodine (30 μM), or the ryanodine receptor antagonist, CPA (20 μM), for 15 min in KRH buffer with or without Ca^{2+} and then assayed for NET activity. The nonspecific signal was defined using 1 μM desipramine. Data represent means±S.E.M. (n=3, n.s. not significant, $^{***}P<0.001$ vs. control in the presence of extracellular Ca^{2+}, Student's t test; $^{###}P<0.001$ vs. control in the extracellular Ca^{2+}-free buffer, ANOVA followed by the Bonferroni method).

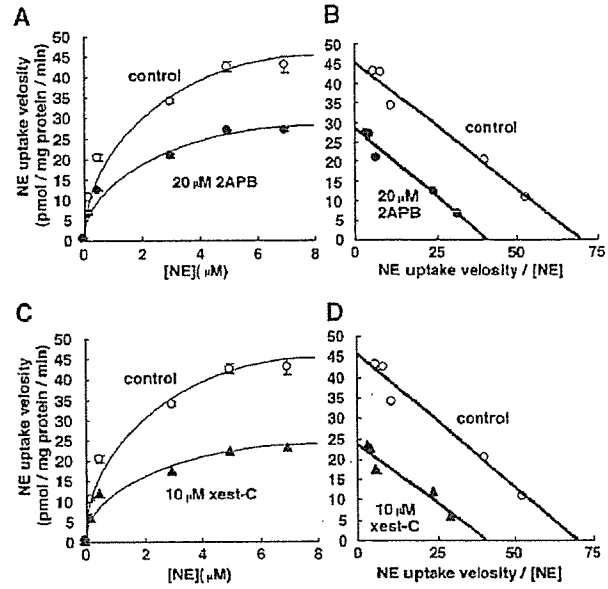

Fig. 4. Effects of IP_3 receptor inhibitors on NET activity are accompanied by a reduction in V_{max}. (A–D) Effects of IP_3 receptor inhibitors on NET activity. Cells were treated with or without 20 μM 2APB or 10 μM xestospongin C (xest-C) for 15 min and then assayed for NET activity (A, C). The data were plotted using the Eadie–Hofstee format, and the V_{max} and K_m values were calculated by linear regression analysis (B, D). The nonspecific signal was defined using 1 μM desipramine.

3.2. IP_3 receptor-dependent release of intracellular Ca^{2+} specifically regulates NET activity

Intracellular Ca^{2+} reportedly has a facilitatory role for NET activity, and chelation of intracellular Ca^{2+} by BAPTA-AM reduces NET activity in SK-N-SH cells (Apparsundaram et al., 2001). We examined the effect of 10 μM BAPTA-AM on NET activity in SH-SY5Y cells. BAPTA-AM reduced NET activity, whereas BAPTA, which is not membrane permeable, did not at an equivalent concentration (Fig. 3A). These results indicate that intracellular Ca^{2+} has a facilitatory role on NET activity in SH-SY5Y cells. Conversely, IP_3 receptor inhibitors block extracellular Ca^{2+} entry via the store-operated Ca^{2+} (SOC) channel (Ma et al., 2000; Van Rossum et al., 2000). The SOC channel becomes activated to replenish intracellular Ca^{2+} stores (Putney, 1986). Thus, the effect of IP_3 receptor inhibitors on NET activity could be a consequence of SOC channel inhibition. To exclude this possibility, we measured norepinephrine uptake in SH-SY5Y cells in the presence of another SOC inhibitor, $LaCl_3$ (Baba et al., 2003). As shown in Fig. 3B, $LaCl_3$ did not alter the NET activity. Moreover, the effect of IP_3 receptor inhibitor was not altered in the presence or absence of extracellular Ca^{2+} (Fig. 3C). These results suggest that the effects of IP_3 receptor inhibitors on NET activity are SOC

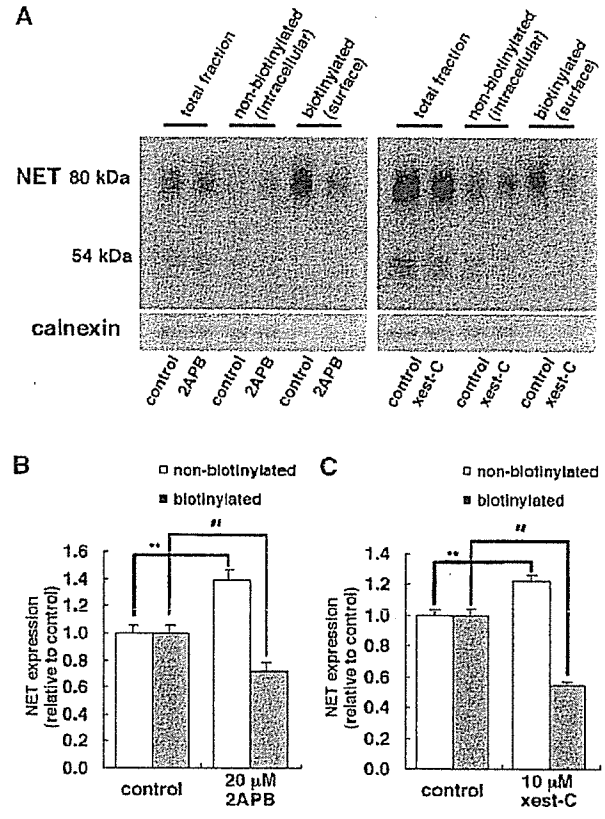

Fig. 5. Effects of IP_3 receptor inhibitors on NET activity are accompanied by a reduction in the surface expression of NET. (A) Analysis of cell surface expression of NET by biotinylation. Following the incubation IP_3 receptor inhibitors, 2APB and xestospongin C, for 15 min, norepinephrine was added (final 500 nM) and incubated for 10 min in KRH buffer prior to biotinylation with sulfo-NHS-LC-biotin (1.5 mg/mL). Cells were lysed with RIPA buffer, and the biotinylated fraction was captured with monomeric avidin beads. Total fraction, non-biotinylated fraction (intracellular), and biotinylated fraction (cell surface) were immunoblotted with anti-NET (1:1000) and anti-calnexin (1:4000). (B, C) Densitometric analysis of non-biotinylated (intracellular) and biotinylated (cell surface) NET expression (80 kDa) shown in A. Data represent means±S.E.M. (n=4 (B), n=3 (C), $^{**}P<0.01$ and $\#\#P<0.01$ v.s. each control, Student's t test).

channel-independent. We also tested whether ryanodine and the ryanodine receptor, another system for intracellular Ca^{2+} release (Berridge et al., 2000), are involved in regulating NET activity. However, treatment with the ryanodine receptor agonist, ryanodine, or antagonist, cyclopiazonic acid (CPA), did not affect NET activity (Fig. 3C), indicating that the release of intracellular Ca^{2+} via IP_3 receptor but not ryanodine receptor is required for the maintenance of NET activity in SH-SY5Y cells.

3.3. The effects of IP_3 receptor inhibitors on NET activity are mediated by a reduction in both V_{max} and surface expression of NET

We analyzed the kinetics of norepinephrine transport in SH-SY5Y cells in the presence or absence of IP_3 receptor inhibitors. Eadie–Hofstee plots showed that treatment with 20 μM 2APB or 10 μM xestospongin C significantly reduced V_{max} from the control level of 45.3±1.35 to 28.5±0.34 pmol/mg protein/min (***$P<0.001$, Student's t test) and 23.4±0.52 pmol/mg protein/min (***$P<0.001$, Student's t test), respectively (Fig. 4A–D). However, the IP_3 receptor inhibitors did not significantly affect K_m values (679.6±6.3 nM to 740.0±35.4 and 620.1±56.5 nM, not significant, Student's t test). The decreased V_{max} values suggest that cell surface expression of functional NET was reduced.

To address this possibility, we assayed for hNET in the total fraction, non-biotinylated fraction (intracellular NET) and biotinylated fraction (NET surface expression) by western blotting using an antibody against hNET. We detected both 80- and 54-kDa forms of hNETs in total and non-biotinylated fraction (Fig. 5A). It is reported that these two forms depend on N-glycosylation of hNET protein (Melikian et al., 1994). Because glycosylation is required for the expression of NET at the cell surface (Nguyen and Amara, 1996), we analyzed 80-kDa of NET. Treatment of SH-SY5Y cells with IP_3 receptor inhibitors increased the expression of intracellular NET and reduced the cell surface expression of NET (Fig. 5A–C). These results suggest that intracellular Ca^{2+} modulation by IP_3 receptor is required to maintain the surface expression of NET. To monitor the efficacy of biotinylation of intracellular proteins, we used calnexin, one of the endoplasmic reticulum marker (Wada et al., 1991). The membrane was reprobed with the anti-calnexin antibody after striping the anti-NET antibody. The results showed the decreased density in biotinylated fraction compared to the total or non-biotinylated fraction (Fig. 5A, lower panel), suggesting that the fractionation was done successfully.

4. Discussion

Although a previous study reported that intracellular Ca^{2+} is involved in NET regulation (Apparsundaram et al., 2001), the detailed mechanism has not been defined. We demonstrated that IP_3 receptor, which controls intracellular Ca^{2+} concentration, regulates NET activity. This is relevant to the function of Ca^{2+} microdomains, which could achieve localized regulation of noradrenergic neurons mediated by NET regulation. We also showed that the IP_3 receptor pathway is involved in regulating the cell surface expression of NET.

IP_3 receptor is activated in parallel with PKC downstream of PLC. It has been reported that PKC activation reduces NET activity (Apparsundaram et al., 1998b). In the present study, the IP_3 receptor inhibitors, 2APB and xestospongin C, reduced NET activity in a dose-dependent manner (Fig. 1), suggesting that the IP_3 receptor–Ca^{2+} system has facilitatory effects on NET activity. The fact that the effect of IP_3 receptor on NET activity is opposite to that of PKC raises the possibility that a balance between these PLC-related signaling pathways is critical for the regulation of NET activity. Another inducer of intracellular Ca^{2+} releaser, ryanodine receptor, as well as an influx of extracellular Ca^{2+} mediated by SOC channels, did not alter NET activity (Fig. 3B,C). Moreover, it has been reported that intracellular Ca^{2+} signaling activated by the muscarinic M_3 receptor reduces NET activity (Apparsundaram et al., 1998a), whereas an influx of extracellular Ca^{2+} induced by the activation of the insulin receptor increases NET activity

(Apparsundaram et al., 2001). These data indicate that the effect of intracellular Ca^{2+} on NET activity is distinct from the sources of Ca^{2+}. Our results suggest that the elevation of NET activity is a consequence of specific intracellular Ca^{2+} release mediated by IP_3 receptor, implying that a specific Ca^{2+} microdomain regulates NET activity. This hypothesis is supported by a report that a Ca^{2+} microdomain involved in IP_3 receptor–Ca^{2+} signaling via the muscarinic M_1 receptor differs from the Ca^{2+} microdomain affected by the bradykinin B_2 receptor in a single cell (Delmas et al., 2002). In fact, the IP_3 receptor inhibitor blocked the elevation of carbachol-stimulated Ca^{2+} concentration (Fig. 2) without decreasing basal (pre-carbachol stimulation) intracellular Ca^{2+} concentration (data not shown). Because intracellular Ca^{2+} is maintained at a low level (about 100 nM) by channels and Ca^{2+}-binding proteins (Berridge et al., 2000), it may be impossible for IP_3 receptor inhibitors to decrease intracellular Ca^{2+} concentration further. On the other hand, these results suggest the possibility that the concentration of Ca^{2+} in a specific Ca^{2+} microdomain relevant to NET activity, which is blocked by IP_3 receptor inhibitors, does not reflect overall intracellular Ca^{2+} concentration. In our study, IP_3 receptor inhibitors reduced NET activity by about 90% (Fig. 1). However, we could not confirm whether BAPTA-AM can abolish NET activity since BAPTA-AM concentrations over 10 μM induced SH-SY5Y cell death (data not shown).

Noradrenergic neurons project over a wide range of the brain, including the cortex, hippocampus, cerebellum and spinal cord (Schroeter et al., 2000). Norepinephrine concentration varies in different regions of the brain (Tanaka et al., 2000). Although localized regulation of each noradrenergic neuron has been suggested (Foote et al., 1983), this mechanism is not clear. NET activity and/or expression level is altered by stimulation of the insulin receptor (Apparsundaram et al., 2001), muscarinic receptor (Apparsundaram et al., 1998a) and nerve growth factor (NGF) receptor (Ikeda et al., 2001). IP_3 receptor functions at the downstream of G-protein-coupled receptors (including the muscarinic receptor) or receptor tyrosine kinases (including the insulin and NGF receptors). These results suggest that extracellular input or the environment alters NET activity, consequently contributing to localized noradrenergic neurotransmission.

We have shown for the first time that IP_3 receptor-mediated intracellular Ca^{2+} has facilitatory effects on NET activity, suggesting that IP_3 receptor-Ca^{2+} signaling functions between NET regulation and signals mediated by cell surface receptors. Since intracellular Ca^{2+} is integral to establishing both temporal and spatial regulation of intracellular signal transduction systems, an IP_3 receptor-mediated Ca^{2+} microdomain may contribute to region-specific regulation of noradrenergic neurons. These findings provide new insights into the regulation of transporters, and the elucidation of the mechanisms underlying the modulation of transporters may lead to novel therapeutic strategies for norepinephrine-related disorders.

Acknowledgment

This work was supported by research grants from the ministry of Health, Labour and Welfare of Japan, the ministry of Education, Culture, Sports, Science and Technology of Japan, and the National Institute of Biomedical Innovation (NIBIO).

References

Apparsundaram, S., Galli, A., DeFelice, L.J., Hartzell, H.C., Blakely, R.D., 1998a. Acute regulation of norepinephrine transport: I. Protein kinase C-linked muscarinic receptors influence transport capacity and transporter density in SK-N-SH cells. J. Pharmacol. Exp. Ther. 287, 733–743.

Apparsundaram, S., Schroeter, S., Giovanetti, E., Blakely, R.D., 1998b. Acute regulation of norepinephrine transport: II. PKC-modulated surface expression of human norepinephrine transporter proteins. J. Pharmacol. Exp. Ther. 287, 744–751.

Apparsundaram, S., Sung, U., Price, R.D., Blakely, R.D., 2001. Trafficking-dependent and -independent pathways of neurotransmitter transporter regulation differentially involving p38 mitogen-activated protein kinase revealed in studies of insulin modulation of norepinephrine transport in SK-N-SH cells. J. Pharmacol. Exp. Ther. 299, 666–677.

Baba, A., Yasui, T., Fujisawa, S., Yamada, R.X., Yamada, M.K., Nishiyama, N., Matsuki, N., Ikegaya, Y., 2003. Activity-evoked capacitative Ca^{2+} entry: implications in synaptic plasticity. J. Neurosci. 23, 7737–7741.

Bauman, A.L., Apparsundaram, S., Ramamoorthy, S., Wadzinski, B.E., Vaughan, R.A., Blakely, R.D., 2000. Cocaine and antidepressant-sensitive biogenic amine transporters exist in regulated complexes with protein phosphatase 2A. J. Neurosci. 20, 7571–7578.

Becherer, U., Moser, T., Stuhmer, W., Oheim, M., 2003. Calcium regulates exocytosis at the level of single vesicles. Nat. Neurosci. 6, 846–853.

Berridge, M.J., Lipp, P., Bootman, M.D., 2000. The versatility and universality of calcium signalling. Nat. Rev., Mol. Cell Biol. 1, 11–21.

Biederman, J., Spencer, T., 1999. Attention-deficit/hyperactivity disorder (ADHD) as a noradrenergic disorder. Biol. Psychiatry 46, 1234–1242.

Brown, R.M., Crane, A.M., Goldman, P.S., 1979. Regional distribution of monoamines in the cerebral cortex and subcortical structures of the rhesus monkey: concentrations and in vivo synthesis rates. Brain Res. 168, 133–150.

Brunello, N., Mendlewicz, J., Kasper, S., Leonard, B., Montgomery, S., Nelson, J., Paykel, E., Versiani, M., Racagni, G., 2002. The role of noradrenaline and selective noradrenaline reuptake inhibition in depression. Eur. Neuropsychopharmacol. 12, 461–475.

Delmas, P., Wanaverbecq, N., Abogadie, F.C., Mistry, M., Brown, D.A., 2002. Signaling microdomains define the specificity of receptor-mediated InsP(3) pathways in neurons. Neuron 34, 209–220.

Foote, S.L., Bloom, F.E., Aston-Jones, G., 1983. Nucleus locus ceruleus: new evidence of anatomical and physiological specificity. Physiol. Rev. 63, 844–914.

Hageman, I., Andersen, H.S., Jorgensen, M.B., 2001. Post-traumatic stress disorder: a review of psychobiology and pharmacotherapy. Acta Psychiatr. Scand. 104, 411–422.

Ikeda, T., Kitayama, S., Morita, K., Dohi, T., 2001. Nerve growth factor down-regulates the expression of norepinephrine transporter in rat pheochromocytoma (PC12) cells. Brain Res. Mol. Brain Res. 86, 90–100.

Kukkonen, J.P., Lund, P.E., Akerman, K.E., 2001. 2-aminoethoxydiphenyl borate reveals heterogeneity in receptor-activated Ca(2+) discharge and store-operated Ca(2+) influx. Cell Calcium 30, 117–129.

Levitt, P., Rakic, P., Goldman-Rakic, P., 1984. Region-specific distribution of catecholamine afferents in primate cerebral cortex: a fluorescence histochemical analysis. J. Comp. Neurol. 227, 23–36.

Ma, H.T., Patterson, R.L., Van Rossum, D.B., Birnbaumer, L., Mikoshiba, K., Gill, D.L., 2000. Requirement of the inositol trisphosphate receptor for activation of store-operated Ca^{2+} channels. Science 287, 1647–1651.

Melikian, H.E., McDonald, J.K., Gu, H., Rudnick, G., Moore, K.R., Blakely, R.D., 1994. Human norepinephrine transporter. Biosynthetic studies using a site-directed polyclonal antibody. J. Biol. Chem. 269, 12290–12297.

Nguyen, T.T., Amara, S.G., 1996. N-linked oligosaccharides are required for cell surface expression of the norepinephrine transporter but do not influence substrate or inhibitor recognition. J. Neurochem. 67, 645–655.

Olivos Ore, L., Artalejo, A.R., 2004. Intracellular Ca^{2+} microdomain-triggered exocytosis in neuroendocrine cells. Trends Neurosci. 27, 113–115.

Pacholczyk, T., Blakely, R.D., Amara, S.G., 1991. Expression cloning of a cocaine- and antidepressant-sensitive human noradrenaline transporter. Nature 350, 350–354.

Putney Jr., J.W., 1986. A model for receptor-regulated calcium entry. Cell Calcium 7, 1–12.

Schroeter, S., Apparsundaram, S., Wiley, R.G., Miner, L.H., Sesack, S.R., Blakely, R.D., 2000. Immunolocalization of the cocaine- and antidepressant-sensitive l-norepinephrine transporter. J. Comp. Neurol. 420, 211–232.

Tanaka, M., 1999. Emotional stress and characteristics of brain noradrenaline release in the rat. Ind. Health 37, 143–156.

Tanaka, M., Yoshida, M., Emoto, H., Ishii, H., 2000. Noradrenaline systems in the hypothalamus, amygdala and locus coeruleus are involved in the provocation of anxiety: basic studies. Eur. J. Pharmacol. 405, 397–406.

Thomas, D.N., Post, R.M., Pert, A., 1994. Focal and systemic cocaine differentially affect extracellular norepinephrine in the locus coeruleus, frontal cortex and hippocampus of the anaesthetized rat. Brain Res. 645, 135–142.

Van Rossum, D.B., Patterson, R.L., Ma, H.T., Gill, D.L., 2000. Ca^{2+} entry mediated by store depletion, *S*-nitrosylation, and TRP3 channels. Comparison of coupling and function. J. Biol. Chem. 275, 28562–28568.

Wada, I., Rindress, D., Cameron, P.H., Ou, W.J., Doherty II, J.J., Louvard, D., Bell, A.W., Dignard, D., Thomas, D.Y., Bergeron, J.J., 1991. SSR alpha and associated calnexin are major calcium binding proteins of the endoplasmic reticulum membrane. J. Biol. Chem. 266, 19599–19610.

Xu, F., Gainetdinov, R.R., Wetsel, W.C., Jones, S.R., Bohn, L.M., Miller, G.W., Wang, Y.M., Caron, M.G., 2000a. Mice lacking the norepinephrine transporter are supersensitive to psychostimulants. Nat. Neurosci. 3, 465–471.

Xu, F., Zhang, J., Recio-Pinto, E., Blanck, T.J., 2000b. Halothane and isoflurane augment depolarization-induced cytosolic Ca^{2+} transients and attenuate carbachol-stimulated Ca^{2+} transients. Anesthesiology 92, 1746–1756.

Zheng, J.Q., 2000. Turning of nerve growth cones induced by localized increases in intracellular calcium ions. Nature 403, 89–93.

BRAIN RESEARCH 1070 (2006) 1–14

available at www.sciencedirect.com

SCIENCE DIRECT

www.elsevier.com/locate/brainres

BRAIN RESEARCH

Research Report

Identification and functional characterization of mouse TPO1 as a myelin membrane protein

Nobuna Fukazawa[a,c,1], Koichi Ayukawa[a,1], Kaori Nishikawa[a], Hiroki Ohashi[a,f], Nobutsune Ichihara[d], Yuki Hikawa[a], Toshiaki Abe[f], Yoshihisa Kudo[c], Hiroshi Kiyama[e], Keiji Wada[a], Shunsuke Aoki[a,b,*]

[a]Department of Degenerative Neurological Diseases, National Institute of Neuroscience, National Center of Neurology and Psychiatry, Kodaira, Tokyo 187-8502, Japan
[b]Department of Demyelinating Disease and Aging, National Institute of Neuroscience, National Center of Neurology and Psychiatry, Kodaira, Tokyo 187-8502, Japan
[c]Laboratory of Cellular Neurobiology, Tokyo University of Pharmacology and Life Science, Hachioji, Tokyo 192-0392, Japan
[d]Department of Anatomy, School of Veterinary Medicine, Azabu University, Sagamihara 229-8501, Japan
[e]Department of Anatomy, Graduate School of Medicine, Osaka City University, Asahimachi, Abenoku, Osaka 545-8585, Japan
[f]Department of Neurosurgery, Jikei University School of Medicine, Minatoku, Tokyo 105-8401, Japan

ARTICLE INFO

Article history:
Accepted 17 November 2005
Available online 6 January 2006

Keywords:
Myelin
Oligodendrocyte
Schwann cell
Fyn
AIGP

ABSTRACT

TPO1 is a member of the AIGP family, a unique group of proteins that contains 11 putative transmembrane domains. Expression of the rat TPO1 gene is upregulated in cultured oligodendrocytes (OLs) during development from pro-oligodendroblasts to postmitotic OLs. However, the distribution of native TPO1 protein in cultured OLs and in the brain has not been elucidated. We investigated the distribution and cellular function of TPO1 in myelinating cells of the nervous system. In mice, TPO1 gene expression was detected in the central (CNS) and peripheral (PNS) nervous systems and was markedly upregulated at postnatal days 10–20, an early phase of myelination in the mouse brain. To investigate TPO1 localization, we generated affinity-purified antibodies to synthetic peptides derived from mouse TPO1. Immunohistochemical analysis showed that TPO1 was expressed in OLs and Schwann cells but not in neurons and astrocytes. Schwann cells from trembler mice, which lack PNS myelin, had significantly decreased TPO1 expression and an altered localization pattern, suggesting that TPO1 is a functional myelin membrane protein. In OL lineage cell cultures, TPO1 was detected in A2B5(+) bipolar early progenitors, A2B5(+) multipolar Pro-OLs, GalC(+) immature OLs and MBP(+) mature OLs. The subcellular localization of TPO1 in OL lineage cells was mapped to the GM130(+) Golgi in cell bodies and Fyn(+) cell processes and myelin-like sheets. Furthermore, TPO1 selectively colocalized with non-phosphorylated Fyn and promoted Fyn autophosphorylation in COS7 cells, suggesting that TPO1 may play a role in myelin formation via Fyn kinase activation in the PNS and CNS.

* Corresponding author. Department of Degenerative Neurological Diseases, National Institute of Neuroscience, National Center of Neurology and Psychiatry, 4-1-1, Ogawahigashi, Kodaira, Tokyo 187-8502, Japan. Fax: +81 42 346 1745.
E-mail address: aokis@ncnp.go.jp (S. Aoki).
[1] These two authors contributed equally to this work.

0006-8993/$ – see front matter © 2005 Elsevier B.V. All rights reserved.
doi:10.1016/j.brainres.2005.11.069

Abbreviations:
aa, amino acid
AIGP, axotomy-induced glycosylated/Golgi-complex protein
CNS, central nervous system
DMEM, Dulbecco's modified Eagle' medium
EEA1, early endosome antigen1
EGFP, enhanced green fluorescent protein
ER, endoplasmic reticulum
GalC, galactocerebroside
GAPDH, glyceraldehyde-3-phosphate dehydrogenase
GFAP, glial fibrillary acidic protein
HRP, horseradish peroxidase
Lamp-1, lysosome-associated membrane glycoprotein-1
MAG, myelin-associated glycoprotein
Map-2, microtubule-associated protein-2
MBP, myelin basic protein
nt, nucleotide
MOG, myelin oligodendrocyte glycoprotein
MyTI, myelin transcriptional factor I
OL, oligodendrocyte
OPC, oligodendrocyte precursor cell
ORF, open reading frame
P0, myelin protein zero
PBS, phosphate-buffered saline
PLP, proteolipid protein
PMP22, peripheral myelin protein-22
PNS, peripheral nervous system
T-TBS, Tris-buffered saline containing 0.1% (v/v) Tween-20

1. Introduction

Schwann cells and oligodendrocytes (OLs) produce myelin in the PNS and CNS, respectively. Myelin is composed of lamellar membranes and ensheaths axons and is essential for nervous system function, as demonstrated by the severe neurological symptoms observed in various myelin diseases (Baumann and Pham-Dinh, 2001; Shy et al., 2002). A number of myelin membrane proteins have been identified to date and have been shown to play pivotal roles in myelin construction and maintenance (Baumann and Pham-Dinh, 2001). Myelin-associated glycoprotein (MAG) is a single transmembrane protein and has multiple immunoglobulin domains, and MAG-deficient mice show delayed myelin compaction (Li et al., 1994). Myelin OL glycoprotein (MOG) is a CNS myelin-specific, single-transmembrane protein that induces experimental autoimmune encephalomyelitis (Scolding et al., 1989; Weissert et al., 1998). Proteolipid protein (PLP) is the most abundant myelin membrane protein, comprising 50% of total myelin protein, and is a member of the tetraspan protein family. Studies in jumpy mice and human Pelizaeus–Merzbacher disease have shown that PLP is essential for stabilizing the myelin membrane (Klugmann et al., 1997; Baumann and Pham-Dinh, 2001). Peripheral myelin protein-22 (PMP22), another member of the tetraspan protein family, and myelin protein zero (P0), a single-transmembrane domain protein, specifically localize to PNS myelin membranes, and the genes encoding these proteins are among those causing Charcot–Marie–Tooth disease (Sakamoto et al., 1987; Lupski et al., 1991; Suter et al., 1992; Suh et al., 1997; Sakai et al., 1999).

AIGP1 (axotomy-induced glycosylated/Golgi complex protein 1) is a neuronal membrane protein that specifically localizes to Golgi membranes in neurons. AIGP1 has eleven potential transmembrane helices. Previously, we reported the possible involvement of AIGP1 in axotomy-associated neuronal cell death (Aoki et al., 2002). The AIGP family genes are evolutionarily conserved from yeast to mammals and, in mammals, consist of three members AIGP1, TMS-2 (Grossman et al., 2000; Aoki et al., 2002) and TPO1 (Krueger et al., 1997). The rat TPO1 gene was originally identified by

differential gene screening, and its expression was shown to be upregulated during OL differentiation (Krueger et al., 1997). Pfeiffer and coworkers also showed that the TPO1 gene is expressed in cultured OLs and rat brain (Krueger et al., 1997). However, the lack of availability of TPO1-specific antibodies has precluded elucidation of the natural distribution and function of this protein. Similarly to other proteins in the AIGP family, TPO1 is also a putative eleven-span membrane protein. However, the putative TPO1 amino acid sequence also has features that distinguish it from other AIGP family members; these features include an extremely polarized structure (N-terminal basic and C-terminal acidic composition), a sequence homologous to myelin transcriptional factor I (MyTI) and a potential C-terminal palmitoylation sequence (Krueger et al., 1997). Accordingly, the cell type-specific expression patterns of TPO1 are distinct from those of the AIGP1 and TMS-2 genes in the nervous system; AIGP1 and TMS-2 are specifically expressed in neurons (Grossman et al., 2000; Aoki et al., 2002), whereas the rat TPO1 gene is expressed in OL lineage cells (Krueger et al., 1997). AIGP1 has been suggested to function as a cell death regulator in axotomized neurons (Aoki et al., 2002), but the biological function of TPO1 is not known.

In this study, we used TPO1-specific antibodies to investigate the localization of TPO1 and to characterize its function in the nervous system. We show that TPO1 is a myelin membrane protein that possibly promotes autophosphorylation of Fyn kinase. Our results suggest that TPO1, a glial subtype of the AIGP family, may play a role in myelin formation and maintenance by regulating Fyn kinase activity.

2. Results

2.1. *Identification of mouse TPO1*

While screening for molecules involved in neuronal regeneration and death, we previously identified a mouse axotomy-induced glycosylated/Golgi complex protein, AIGP1 (Grossman et al., 2000; Aoki et al., 2002). Database searches suggested that the mouse or rat genome encodes three AIGP1 homologs: AIGP1, TMS-2 (GenBank accession no. AF181685) and TPO1 (GenBank accession no. L20319) (Fig. 1A). In mice, the AIGP1 and TMS-2 genes are expressed in neurons in the cortex, hippocampus, cerebellum and hypoglossal nucleus (Grossman et al., 2000; Aoki et al., 2002). On the other hand, in rats, the TPO1 gene has been reported to be expressed in OL lineage cells in vitro (Krueger et al., 1997). Since the cell type-specific expression pattern of TPO1 suggests distinct functionality, we were interested in the molecular function of TPO1 in the nervous system. The mouse TPO1 cDNA sequence (GenBank accession no. AB029501, (Aoki et al., 2002)) contains a 1416-bp open reading frame (ORF) that is homologous to the rat TPO1 cDNA sequence (57.7%). The ORF encodes 462 aa with 90% similarity to rat TPO1. Mouse AIGP1 and TMS-2 are less similar (36.8% and 39%, respectively) to mouse TPO1 (data not shown). The sequence of TPO1 is less conserved compared with AIGP1 and TMS-2 (Grossman et al., 2000; Aoki et al., 2002). Computational analyses with the transmembrane prediction software SOSUI (http://sosui.proteome.bio.tuat.ac.jp) suggest that TPO1 has eleven putative transmembrane helices (Fig. 1B). The second and fourth extracellular loops and fifth intracellular loop have relatively longer structures than the other loops (Fig. 1B), but the amino acid sequences of the long loops are not well conserved between TPO1 and other family members (data not shown). Two cysteine-rich zinc finger-like motifs, $CX_5CX_{6-10}CX_2C$ (residues 6–27, similar to aminoacyl tRNA synthetases) and $CX_5CX_1CX_4H$ (residues 100–123, similar to transcription factor MYT1; (Hirayama et al., 2003), and a potential C-terminal palmitoylation sequence (residues 453–454) were also found in the TPO1 sequence (Fig. 1B, Krueger et al., 1997). These motifs are highly conserved between rats and mice, but are not present in mouse AIGP1 and TMS-2 (data not shown). Two potential N-linked glycosylation sites (Asn-X-Thr) were identified in both AIGP1 and TMS-2 (Grossman et al., 2000; Aoki et al., 2002), but such sites were not found in the amino acid sequence of TPO1 (data not shown). Two potential phosphorylation sites for protein kinase C were identified in the second and third intracellular loops, and one potential target site for cAMP-dependent protein kinase was found in the fifth intracellular loop of TPO1 (data not shown). Phylogenetic analysis of the AIGP family members showed that mouse and rat TPO1 form a cluster that is completely separate from the AIGP1 and TMS-2 clusters (Fig. 1A).

2.2. *TPO1 expression in the PNS and CNS*

Previous studies (Krueger et al., 1997) have shown that the rat TPO1 gene is expressed in the CNS and in OL lineage cells. To examine gene expression levels in the PNS and CNS precisely, we performed SYBR green-based real-time RT-PCR analysis with the mouse CNS and PNS myelin-specific markers MOG (Scolding et al., 1989) and P0 (Sakamoto et al., 1987; Lupski et al., 1991) (Fig. 1C, top). We examined TPO1 gene expression in the mouse dorsal root ganglion and brain. Both PNS and CNS tissues expressed TPO1 mRNA at considerable levels, which were remarkably higher than expression levels observed in the E14 brain (Fig. 1C, top). In the postnatal CNS, TPO1 gene expression markedly increased after P10 and reached a maximum level at P20. This level of expression was maintained throughout adult life (Fig. 1C, bottom).

2.3. *Production and characterization of antibodies to mouse TPO1*

We prepared specific antibodies against relatively hydrophilic peptide sequences of the fifth intracellular and second extracellular loops of mouse TPO1 (EP05 and EP06, respectively, [EP; epitope], Fig. 1B). Immunoblot analysis using mouse cultured OL cell lysates showed that anti-TPO1 (ABEP05; against EP05) recognized a ~48-kDa band (Fig. 2A, lane 2) that was slightly smaller than the expected molecular mass (51.8 kDa), probably because of its hydrophobicity (Fig. 2A, lane 2). No signal was detected when the blot was probed with control rabbit IgG (Fig. 2A, lanes 3 and 4). TPO1 was detected in the membrane fraction but not in the soluble fraction (Fig. 2A, lanes 1 and 2).

2.4. *Localization of TPO1 in the mouse PNS and CNS tissues*

To determine the localization of mouse TPO1 in the PNS and CNS, immunohistochemical analyses were performed with the TPO1-specific antibody, ABEP05. Mouse sciatic nerves and cerebellar medulla both showed myelin-like immunoreactivity (Figs. 2B, b–d), whereas staining with negative control rabbit IgG at the same concentration yielded no signal (Figs. 2B, a). TPO1 specifically localized to the OL-enriched regions in the CNS, including white matter tracts in the cerebrum, caudate–putamen (Figs. 2C, b and c) and cerebellum (Figs. 2C, e and f). Pre-absorption of ABEP05 with the epitope peptide EP05 abrogated the cerebrum signals (Figs. 2C, a), indicating that anti-TPO1 specifically recognized mouse TPO1 in vivo.

To determine the cell type-specific expression of TPO1 in the nervous system, we double-stained brain sections of adult mouse with anti-TPO1 and cell type-specific marker antibodies, including anti-MBP as a marker of both Schwann cells and OLs, anti-Map-2 as a neuron marker, and anti-GFAP as an astrocyte marker. TPO1 staining colocalized with MBP staining in the sciatic nerve (Figs. 3A a–c), white matter tracts of the cerebrum (Figs. 3B, a–c) and cerebellum (Figs. 3B d–f), but the staining did not overlap with that of Map-2 (Figs. 3C, a–c) or GFAP (Figs. 3C, d–f). In the cerebellum, TPO1 staining also overlapped with O4 staining (Figs. 3C, g–i). These data suggest that TPO1 localizes specifically to Schwann cells and OLs in the PNS and CNS, respectively.

2.5. *Mislocalized and decreased expression of mouse TPO1 in the PNS myelin membrane of the trembler-Ncnp mouse*

To confirm the specific expression of TPO1 in myelin-producing cells and to address whether it specifically

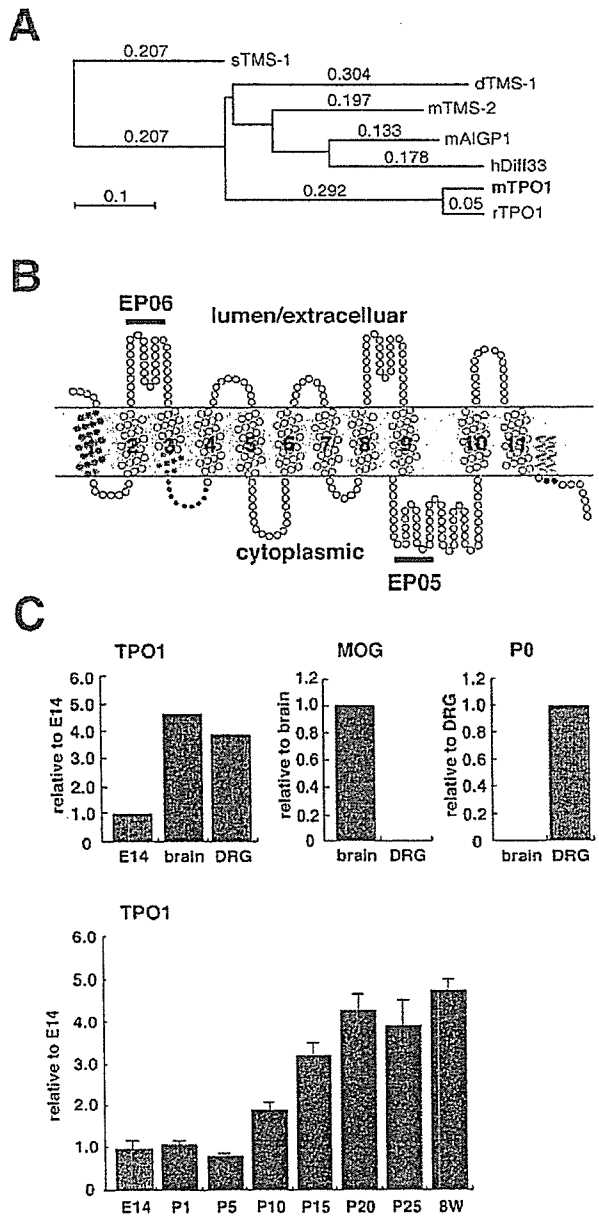

localizes to the myelin membrane in vivo, we examined the expression pattern of TPO1 in the sciatic nerve of adult trembler-Ncnp mice, which exhibit specific loss of MBP-positive myelin membranes in Schwann cells (Suh et al., 1997; Sakai et al., 1999). MBP staining was completely absent from the myelin in the sciatic nerve of trembler-Ncnp mice (Figs. 4A, e), indicating the loss of myelin membrane, whereas intact MBP-positive myelin membrane was detectable in wild-type mice (Figs. 4A, b). TPO1 staining was markedly decreased in trembler-Ncnp mice compared with wild-type mice (Figs. 4A, a and d; B, a and b), and small puncta of TPO1 staining remained in Schwann cells (Figs. 4B, b; arrowheads). These results clearly indicate that TPO1 is a myelin membrane protein in Schwann cells.

2.6. *Expression of TPO1 in OL lineage cells*

TPO1 staining colocalized with MBP staining in the PNS and CNS (Fig. 3), suggesting its specific localization in OLs and Schwann cells. Moreover, the loss of TPO1 staining in the sciatic nerve tissue of trembler-Ncnp mice indicated its specific localization to PNS myelin membranes (Fig. 4). However, gross immunostaining analyses of the CNS were not sufficient to confirm the localization of TPO1 in OLs. To test whether TPO1 is specifically expressed in OLs in the CNS, we performed immunostaining with anti-TPO1 in various types of cells isolated from the CNS, including mouse embryonic cortical neuroepithelial cells, rat optic nerve-derived OL lineage cells, mouse cortical neurons and astrocytes. TPO1 staining was not detectable in nestin (+) neuroepithelial cells (Figs. 5A, H and O). However, a small number of TPO1-expressing cells were detected in neuroepithelial cell cultures (Figs. 5A, H and O), and these cells are likely to be differentiated cells derived from neuroepithelial cells because of the absence of, or decrease in, nestin expression (Figs. 5A, H and O, arrowhead). The rat optic nerve-derived OL lineage cells, including A2B5(+) bipolar early progenitors (Figs. 5B, I and P), A2B5(+) multipolar Pro-OLs (Figs. 5C, J and Q), GalC(+) immature OLs (Figs. 5D, K and R) and MBP(+) mature OLs (Figs. 5E, L and S) all expressed TPO1. Map2(+) neurons and GFAP(+) astrocytes cultured in vitro showed no TPO1 staining (Figs. 5F, G, M, N, T, and U), in good agreement with the results of immunohistochemical analyses in intact tissues (Figs. 3C, a–f). Immunostaining with negative control IgG yielded no specific staining, and pre-adsorption of anti-TPO1 with antigen peptide abolished staining (data not shown).

2.7. *Subcellular localization of TPO1 in the Golgi and myelin in OLs*

To determine the subcellular localization of TPO1 in OLs, rat optic nerve-derived OLs were double labeled with organelle-specific markers, and confocal laser scan analyses were performed through all cell structures from the cell bodies (top) through cell processes and myelin-like sheets (bottom). TPO1 staining clearly overlapped with GM130 (Nakamura et al., 1995) staining in cell bodies (Figs. 6A, d, e and f), indicating localization to the Golgi complex in OL cell bodies. However, TPO1 staining did not overlap with that of other markers, including the endoplasmic reticulum marker KDEL (Vaux et al., 1990) (Figs. 6A, a, b and c) in cell bodies, and the lysosomal marker Lamp-1 (Chen et al., 1985) (Figs. 6B, a, b and c), the secretary vesicle marker Rab3a (Fukuda et al., 2002) (Figs. 6B, d, e and f) or the endosome marker EEA1 (Mu et al., 1995) (Figs. 6B, g, h and i) in cell processes and in myelin-like sheets.

TPO1 was expressed in OL lineage cells from early to terminal differentiation stages (Figs. 5B–E). We found that TPO1 staining overlapped with GalC staining in mature OLs (Figs. 6C a–c). The overlapping expression patterns suggested that TPO1 is a constituent of myelin membranes. TPO1 has cysteine residues at the C terminus, which is potentially palmitoylated (Krueger et al., 1997). Fyn tyrosine kinase (Fyn) has also been reported to be palmitoylated (Shenoy-Scaria et al., 1993; Koegl et al., 1994; Wolven et al., 1997) and is important for morphogenesis and myelin formation in OLs (Osterhout et al., 1999; Sperber and McMorris, 2001; Klein et al., 2002; Colognato et al., 2004; Liang et al., 2004). To determine the spatial relationship between TPO1 and Fyn, we double

Fig. 1 – Evolution, structure, and expression profile of mouse TPO1. (A) Phylogeny of amino acid sequences of AIGP family members. Multiple sequence alignment was generated using Clustal W software (Oxford Molecular Group plc, Oxford, UK), and the phylogenic tree was constructed from multiple sequence alignments using the neighbor-joining method with MacVector 7.0 (Oxford Molecular Group plc, Oxford, UK). The length of the horizontal lines indicates relative sequence divergence, and bootstrap probabilities are shown at each node. sTMS-1, *Saccharomyces cerevisiae* TMS-1 (Z47746); dTMS, *Drosophila melanogaster* TMS-1 (AF181686); mAIGP1, mouse AIGP1 (AB029499); mTMS-2, mouse TMS-2 (AF181685); hDiff33, human Diff33 (U49188); rTPO1, rat TPO1 (L20319). (B) Membrane topological model for TPO1. The model illustrates the predicted transmembrane domain and the extra- and intracellular loops. Each circle represents an amino acid, and transmembrane helices are numbered. Cysteine-rich motifs, $CX_5CX_{6-10}CX_2C$ (residues 6–27), are shown as red circles, and zinc-finger-like motifs, $CX_5CX_1CX_4H$ (residues 100–123), are shown in green. The potential C-terminal palmitoylation sequence (residues 453–454) is shown in cyan. EP05 (epitope 05) and EP06 (epitope 06) indicate the peptide antigens used for producing antibodies against mouse TPO1. (C) Gene expression profiles of mouse TPO1. Total RNA was isolated from whole heads of E14 mouse embryos, postnatal whole brains (P1–8 weeks) and dorsal root ganglia (DRG). Each cDNA was synthesized using an equal amount of total RNA. SYBR Green-based quantitative RT-PCR analysis of TPO1 transcripts in the mouse CNS and PNS was performed (top). The β-actin gene was used to normalize the intensities between samples and the MOG and P0 genes were used as controls for CNS- and PNS-specific genes, respectively. The relative gene expression levels from the mice brain and DRG are shown in comparison with the average expression level from E14 heads. The expression levels of TPO1 mRNA during mouse brain development are also shown (bottom). The relative gene expression levels of postnatal developing brains (P1–8 weeks) are shown in comparison with E14 heads. The β-actin gene was used as a calibrator. Each bar represents the mean ± SEM ($n = 3$; three heads or brains).

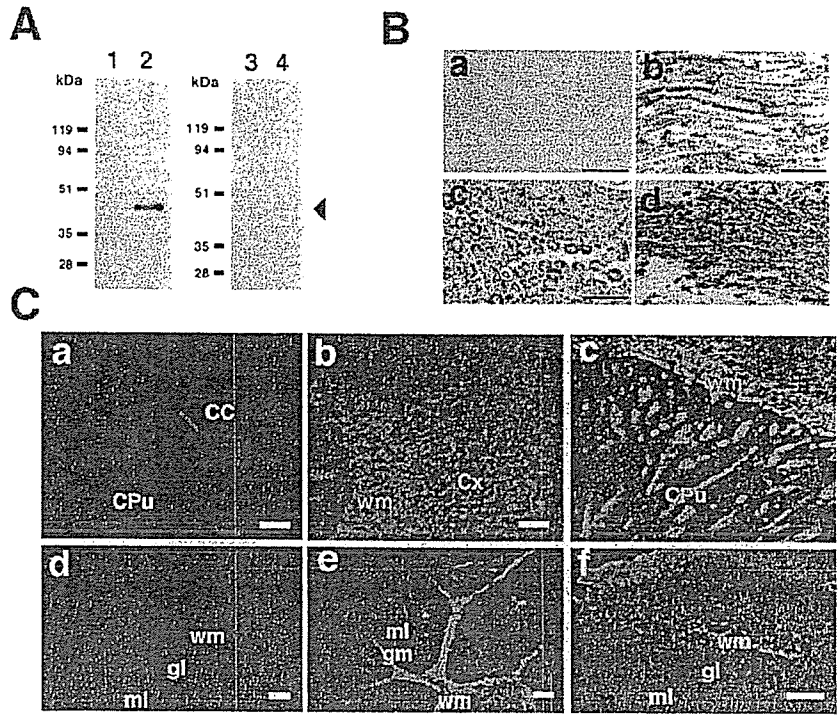

Fig. 2 – Localization of TPO1 in the PNS and CNS. (A) Immunoblot analysis of the soluble and insoluble fractions of OL-derived cell lysates using anti-TPO1 (ABEP05). OLs were lysed with detergent (–) buffer and separated into soluble and insoluble fractions. Soluble (lanes 1 and 3) and insoluble (lanes 2 and 4) fractions were subjected to SDS-PAGE and probed with anti-TPO1 (lanes 1 and 2) or normal rabbit IgG (lanes 3 and 4). The arrowhead indicates the apparent 48 kDa band corresponding to TPO1. (B) Immunohistochemical analyses of TPO1 in the PNS and CNS. Sections (paraffin; 5 μm thickness) were stained with anti-TPO1 (ABEP05; b–d) or normal rabbit IgG (a). Staining was visualized using the diaminobenzidine (DAB) method. Longitudinal (b) and transverse (c) sections of the sciatic nerve are shown. Staining of the cerebellar medulla is shown in d. Scale bars = 40 μm. (C) Localization of TPO1 in the mouse cerebrum (a–c) and cerebellum (d–f). Sagittal frozen sections (20 μm thickness) from P20 mouse brain were immunostained with anti-TPO1 (ABEP05; b, c, e and f). Staining with pre-absorbed antibody (epitope peptide 05; EP05) or normal rabbit IgG are shown in a and d, respectively. Images were obtained by confocal microscopy. CC, corpus callosum; Cx, cortex; CPu, caudate–putamen; ml, molecular cell layer; gl, granule cell layer; wm, white matter. Scale bars = 50 μm.

labeled OLs with antibodies against TPO1 and Fyn. TPO1 partially colocalized with Fyn in a punctate pattern within OL cell processes and myelin membranes (Figs. 6C d, e and f, and C 1 and 2, arrows).

2.8. *TPO1 predominantly colocalizes with non-phosphorylated Fyn tyrosine kinase, and may promote its phosphorylation*

To determine whether TPO1 is involved in the regulation of Fyn tyrosine kinase activity, the phosphorylation levels of Fyn and Src were analyzed in COS7 cells transfected with EGFP-TPO1 or EGFP expression constructs. Immunoblotting with anti-phospho-Src family protein antibodies (specifically recognizing both phospho-Tyr 420 of Fyn and phospho-Tyr 416 of Src) showed an elevated level (over twofold) of phosphorylated Fyn in COS7 cells transfected with EGFP-TPO1 compared with EGFP-transfected cells (Figs. 7I and K, left). The Src phosphorylation level was comparable between EGFP-TPO1- and EGFP-transfected cells (Figs. 7J and K, right). The amount of Fyn, Src and GAPDH (for internal control) protein was equivalent in all samples (Figs. 7I and J), indicating that the elevated level of phosphorylated Fyn was not due to a change in the amount of each protein per cell. While EGFP fluorescence in COS7 cells was uniformly distributed in the cytosol and nucleus, TPO1-EGFP localized to perinuclear Golgi complexes and pericellular puncta (Figs. 7C, D, G and H). In cells doubly transfected with Fyn and TPO1-EGFP constructs, the localization patterns of both proteins partially overlapped (Fig. 7G, arrowhead, and G', arrows), but phosphorylated Fyn was completely segregated from TPO1 (Fig. 7H; arrowheads). This suggests that TPO1 predominantly colocalizes with non-phosphorylated Fyn and not with phosphorylated Fyn. Moreover, EGFP-TPO1-transfected cells showed increased staining for phosphorylated Fyn in pericellular regions (Fig. 7H; arrowheads) compared with EGFP-transfected cells (Fig. 7F), in good agreement with the results from immunoblot analyses (Figs. 7I and K, left). We failed to detect a complex containing TPO1 and Fyn using the immunoprecipitation assay; this was most likely a consequence of the fact that TPO1 is extremely hydrophobic and thus was not solubilized by detergents that is generally used in immunoprecipitation assays.

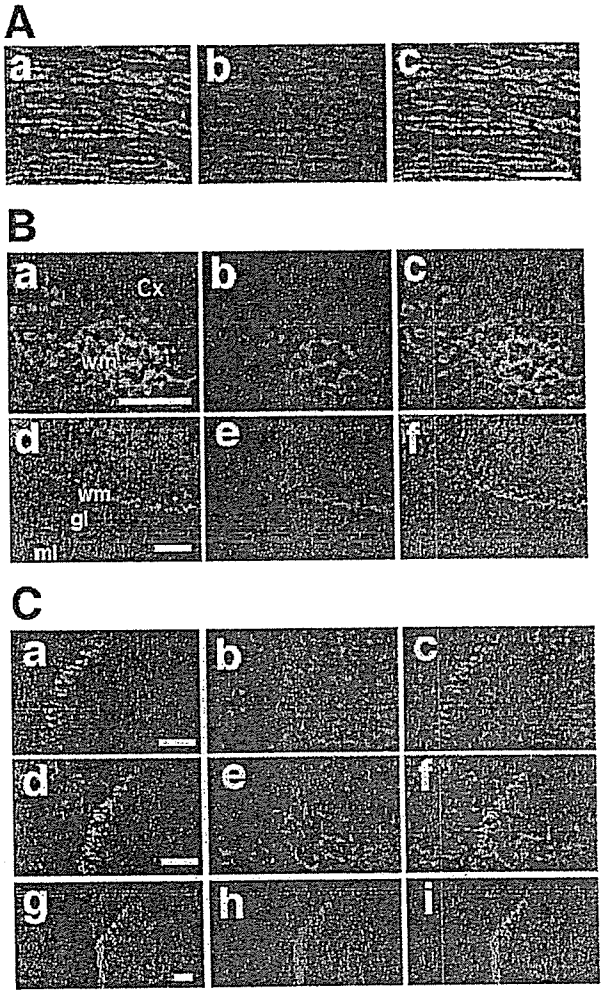

Fig. 3 – Schwann cell- and OL-specific expression of TPO1. Immunofluorescence microscopy of longitudinal sections of the mouse sciatic nerve (A; paraffin; 5 μm thickness), cerebrum (Ba–c) and cerebellum (Bd–f) (frozen section; 20 μm thickness). A and B show staining results as follows: anti-TPO1 (ABEP05; green, A-a and B-a and B-d) and anti-MBP (red, A-b and B-b and B-e). Merged images are shown in A-c and B-c and B-f). Scale bar = 40 μm in A and 50 μm in B. (C) Immunofluorescence microscopy of cerebellum frozen sections (20 μm thickness) stained with neuronal or glial cell markers: anti-TPO1 (ABEP05; a, d and g) and anti-Map2 for neurons (b), anti-GFAP for astrocytes (e), and O4 for OLs (h). Merged images are indicated on the extreme right of each row (c, f and i). Images were obtained by confocal microscopy. Scale bars = 50 μm. Cx, cortex; ml, molecular cell layer; gl, granule cell layer; wm, white matter.

2.9. *MAG cross-linking-induced assembly of TPO1 protein*

Cross-linking of cell surface MAG by a MAG-specific antibody is known to induce tyrosine phosphorylation of Fyn; moreover, the MAG–Fyn pathway is involved in the initial events of myelination (Umemori et al., 1994). To examine whether TPO1 is involved in the MAG–Fyn pathway, we performed a MAG cross-linking experiment in OL-lineage cells. Small dot-like TPO1 signals increased within 30 min in immature OLs treated with anti-MAG IgG (Fig. 8A) in comparison with control IgG (Fig. 8B). Quantitative analysis showed that the number of TPO1-immunoreactive dot-like signals significantly increased by twofold in MAG cross-linked immature OLs (anti-MAG IgG = 136.9 ± 18.73 vs. control IgG = 67.9 ± 8.35, $P < 0.001$, $n = 21$ cells; Fig. 8C). These results suggested that MAG cross-linking altered TPO1 localization via oligomerization of cell surface MAG and that TPO1 is involved in MAG-mediated signaling.

3. Discussion

We have characterized the distribution of TPO1, a new myelin membrane protein of the AIGP family. Previous studies have analyzed expression of the TPO1 gene (Krueger et al., 1997). However, the precise distribution of the protein has not been defined due to the lack of suitable TPO1-specific antibodies, probably because this protein is extremely hydrophobic (average hydrophobicity = 0.39, calculated by the Kyte and

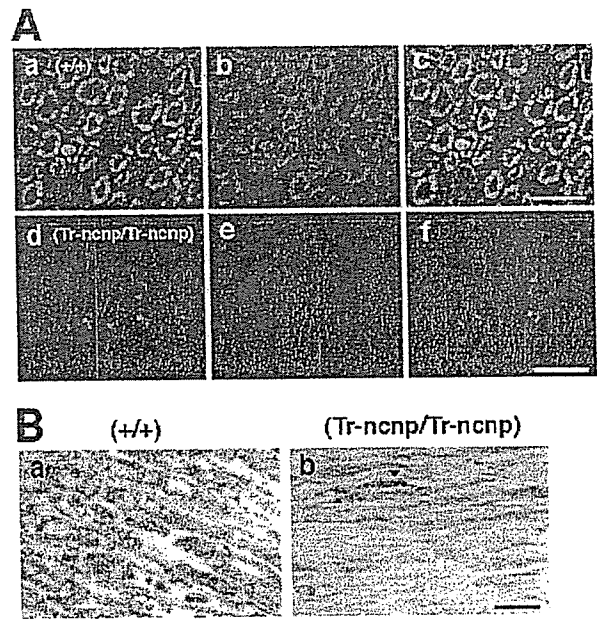

Fig. 4 – Altered expression pattern of TPO1 in the sciatic nerves of trembler mice. (A) Transverse sections (paraffin; 5 μm thickness) of sciatic nerves from adult wild-type (upper images) or trembler-Ncnp mice (lower images). MBP (b, e) was used as a myelin membrane marker in double-labeling experiments with anti-TPO1 (ABEP05; a, d). Merged images are shown in c and f. TPO1 staining in the sciatic nerves was detected in Schwann cell myelin membranes and was decreased in trembler mice. Images were obtained using a CCD camera. Scale bars = 40 μm. (B) Longitudinal section of sciatic nerves from adult wild-type (left) or trembler mice (right). Sections (paraffin; 5 μm thickness) were stained with anti-TPO1 (ABEP05) and were visualized with diaminobenzidine (DAB) and methylene blue for nuclei. TPO1-positive aggregates were observed (b, arrowhead). Scale bars = 20 μm.